Journal of
Composites Science

IMPACT FACTOR 3.7

CITESCORE 5.8

Article

Electrospinning Technology to Influence Hep-G2 Cell Growth on PVDF Fiber Mats as Medical Scaffolds: A New Perspective of Advanced Biomaterial

Héctor Herrera Hernández, Carlos O. González Morán, Gemima Lara Hernández, Ilse Z. Ramírez-León, Citlalli J. Trujillo Romero, Juan A. Alcántara Cárdenas and Jose de Jesus Agustin Flores Cuautle

Special Issue
Sustainable Biocomposites, 3rd Edition

Edited by
Prof. Dr. Ahmed Koubaa, Dr. Mohamed Ragoubi, Dr. Frédéric Becquart, Dr. Ahmed Elloumi and Prof. Dr. Philippe Michaud

MDPI

https://doi.org/10.3390/jcs9080401

Journal of
Composites Science

MDPI

Article

Electrospinning Technology to Influence Hep-G2 Cell Growth on PVDF Fiber Mats as Medical Scaffolds: A New Perspective of Advanced Biomaterial

Héctor Herrera Hernández [1,*], Carlos O. González Morán [2], Gemima Lara Hernández [3], Ilse Z. Ramírez-León [2,†], Citlalli J. Trujillo Romero [4], Juan A. Alcántara Cárdenas [5] and Jose de Jesus Agustin Flores Cuautle [6,*]

1 Laboratorio de Investigación en Electroquímica y Corrosión de Materiales Industriales, Universidad Autónoma del Estado de México, Blvd. Universitario s/n, Predio San Javier, Atizapán de Zaragoza 54500, Mexico
2 Laboratorio de Investigación de Materiales y Procesos Inteligentes, Universidad Autónoma del Estado de México, Blvd. Universitario s/n, Predio San Javier, Atizapán de Zaragoza 54500, Mexico; cogonzalezm@uaemex.mx (C.O.G.M.); zuryleon13@gmail.com (I.Z.R.-L.)
3 Tecnológico Nacional de México, Instituto Tecnológico de Orizaba, Oriente 9, Orizaba 94320, Mexico; larag_139@hotmail.com
4 Laboratorio de Biomecánica, Instituto Nacional de Rehabilitación-LGII, Calzada Xochimilco 289, Colonia Arenal de Guadalupe, Tlalpan, Ciudad de México 14389, Mexico; cjtrujillo@inr.gob.mx
5 Centro Interdisciplinario de Investigaciones y Estudios sobre Medio Ambiente y Desarrollo (CIIEMAD), Instituto Politécnico Nacional (IPN), Ticomán, Gustavo A. Madero, Ciudad de México 07340, Mexico; e-jaalcantarac@ipn.mx
6 Secihti-Tecnológico Nacional de México, Instituto Tecnológico de Orizaba, Centro Universitario UAEM Valle de México, Oriente 9, Orizaba 94320, Mexico
* Correspondence: hherrerah@uaemex.mx (H.H.H.); jflores_cuautle@hotmail.com (J.d.J.A.F.C.)
† Engineering student.

Academic Editors: Ahmed Koubaa, Mohamed Ragoubi, Frédéric Becquart, Ahmed Elloumi and Philippe Michaud

Received: 26 June 2025
Revised: 23 July 2025
Accepted: 28 July 2025
Published: 1 August 2025

Citation: Herrera Hernández, H.; González Morán, C.O.; Lara Hernández, G.; Ramírez-León, I.Z.; Trujillo Romero, C.J.; Alcántara Cárdenas, J.A.; Flores Cuautle, J.d.J.A. Electrospinning Technology to Influence Hep-G2 Cell Growth on PVDF Fiber Mats as Medical Scaffolds: A New Perspective of Advanced Biomaterial. *J. Compos. Sci.* **2025**, *9*, 401. https://doi.org/10.3390/jcs9080401

Abstract

This research focuses on designing polymer membranes as biocompatible materials using home-built electrospinning equipment, offering alternative solutions for tissue regeneration applications. This technological development supports cell growth on biomaterial substrates, including hepatocellular carcinoma (Hep-G2) cells. This work researches the compatibility of polymer membranes (fiber mats) made of polyvinylidene difluoride (PVDF) for possible use in cellular engineering. A standard culture medium was employed to support the proliferation of Hep-G2 cells under controlled conditions (37 °C, 4.8% CO_2, and 100% relative humidity). Subsequently, after the incubation period, electrochemical impedance spectroscopy (EIS) assays were conducted in a physiological environment to characterize the electrical cellular response, providing insights into the biocompatibility of the material. Scanning electron microscopy (SEM) was employed to evaluate cell adhesion, morphology, and growth on the PVDF polymer membranes. The results suggest that PVDF polymer membranes can be successfully produced through electrospinning technology, resulting in the formation of a dipole structure, including the possible presence of a polar β-phase, contributing to piezoelectric activity. EIS measurements, based on R_{ct} and C_{dl} values, are indicators of ion charge transfer and strong electrical interactions at the membrane interface. These findings suggest a favorable environment for cell proliferation, thereby enhancing cellular interactions at the fiber interface within the electrolyte. SEM observations displayed a consistent distribution of fibers with a distinctive spherical agglomeration on the entire PVDF surface. Finally, integrating piezoelectric properties into cell culture systems provides new opportunities for investigating the influence of electrical interactions on cellular behavior through electrochemical techniques. Based on the experimental results, this electrospun polymer demonstrates great potential as a promising candidate for next-generation biomaterials, with a probable application in tissue regeneration.

Keywords: Hep-G2; culture cell; PVDF fiber mats; electrochemical impedance; electrospinning technology

1. Introduction

Cell growth is a regulated biological process resulting from a precise equilibrium between cellular proliferation and degradation and the complex and dynamic interactions between cells and the extracellular matrix (ECM). The ECM is a three-dimensional network composed of structural proteins and hydrated polysaccharide compounds, providing mechanical support and biochemical interactions. These interactions are essential for maintaining cellular function and tissue homeostasis conditions, involving a wide range of morphological, biochemical, biophysical, and bioelectrical mechanisms. In scaffold-based tissue engineering, it is fundamental to characterize and optimize the cellular growth rate for each specific scaffold design. One of the main challenges in studying ECM–cell interactions stems from the complexity of the interface phenomena, including cellular adhesion, phenotype differentiation, signal transduction, and mechanobiological responses [1–3]. Among the biophysical interactions, the piezoelectric effect is particularly noteworthy for its ability to convert mechanical stimuli into electrical signals, influencing intracellular signaling pathways and regulating cellular processes of interest. This electromechanical transduction plays a critical role in mechanosensing, bone remodeling, and cellular orientation, functions that are especially significant in scaffolds designed to mimic native tissue environments.

It is worth mentioning that incorporating piezoelectric properties into biomaterials enhances their functional capabilities, offering advanced strategies for the development of intelligent scaffolds for tissue engineering and regenerative medicine [4,5]. One such material is polyvinylidene difluoride (PVDF), a highly versatile and electroactive polymer widely studied for its unique properties. The molecular structure of PVDF consists of repeating $(CH_2\text{-}CF_2)_n$ units, where the number of repeating units (n) determines the polymer chain length, which in turn influences its crystallinity and physical behavior. The presence of highly electronegative fluorine atoms results in strong polar C–F bonds with significant dipole moments, conferring PVDF its excellent piezoelectric characteristics. In addition to its electroactivity, PVDF offers high mechanical strength, exceptional chemical and thermal stability, as well as excellent flexibility and biocompatibility. It is non-biodegradable and corrosion-resistant under certain environmental conditions, making it suitable for long-term biomedical applications [3,6]. PVDF can exist in several crystalline phases, including non-polar α- and ε-phases and polar β-, γ-, and δ-phases. Among these, the β-phase is the most electroactive due to its all-trans planar zigzag conformation structure, in which all dipole moments are aligned in the same direction [6–9]. This arrangement maximizes spontaneous polarization and is responsible for PVDF's outstanding piezoelectric behavior. The β-phase can be induced through various physical and chemical processes, including mechanical stretching, electrical poling, or advanced fabrication techniques like electrospinning. Electrospinning enhances β-phase formation by applying high electric fields and intense elongational forces to the polymer jet, aligning molecular chains and promoting crystallization of the electroactive phase. This technique increases the proportion of the β-phase and produces nanofibrous mats with a high surface area, porosity, and mechanical flexibility. These features closely mimic the natural ECM, making PVDF electrospun mats ideal for medical applications [10,11].

In previous studies, authors have demonstrated that polyvinylidene fluoride (PVDF) is a high-performance polymer known for its superior electroactive properties, primarily

attributed to the polar β-phase, which adopts a specific molecular arrangement where dipoles are aligned, resulting in a material with strong piezoelectric properties [12,13]. Electrospinning has been extensively applied to PVDF processing, promoting β-phase formation through high-voltage-induced stretching and solvent evaporation, enabling the fabrication of highly aligned nanofibrous mats without post-treatment [14]. These nanofibers offer not only mechanical strength and flexibility, but also excellent biocompatibility and enhanced interfacial electrical interactions, making them promising candidates for tissue regeneration platforms [15]. In comparison, traditional electroactive polymers such as polypyrrole (PPy) and polyaniline (PANI) have been explored for similar applications due to their intrinsic conductivity; however, they often suffer from significant disadvantages, including poor mechanical properties, limited flexibility, and lower long-term biocompatibility [16]. Additionally, commonly used biodegradable polymers such as polylactic acid (PLA), polycaprolactone (PCL), and polyglycolic acid (PGA) demonstrate excellent biodegradability but lack inherent electrical activity, which restricts their application in electrically responsive biomedical systems. Compared to these materials, PVDF offers a unique combination of mechanical robustness, electrical functionality, and biological compatibility, positioning it as a superior option for multifunctional biomaterials in tissue engineering [17]. A comparative summary of the characteristics of these polymers, including PVDF, is presented in Table 1.

Table 1. Comparative summary of applied polymers in biomedical engineering, focusing on their chemical structure, applications, and functional properties, including PVDF [6–17].

Polymer	Chemical Formula	Principal Applications	Significant Properties
PVDF (Polyvinylidene fluoride)	$(C_2H_2F_2)_n$	Sensors, energy collectors, tissue engineering	High chemical stability, piezoelectricity (β-phase), excellent biocompatibility
PPy (Polypyrrole)	$(C_4H_3N)_n$	Biosensors, drug delivery, neural interfaces	Intrinsic conductivity, poor mechanical flexibility, limited biodegradability
PANI (Polyaniline)	$(C_6H_5NH)_n$	Conductive coatings, sensors, neural electrodes	Conductive, environmental instability, poor mechanical strength
PLA (Polylactic acid)	$(C_3H_4O_2)_n$	Biodegradable scaffolds, medical implants	Biodegradable, good mechanical properties, lacks electrical activity
PCL (Polycaprolactone)	$(C_6H_{10}O_2)_n$	Long-term implants, drug delivery	Slow biodegradation, flexible, electrically inert
PGA (Polyglycolic acid)	$(C_2H_2O_2)_n$	Fast-degrading sutures, tissue scaffolds	Rapid biodegradation, good strength, no piezoelectricity

In tissue regeneration, PVDF-based mats offer unique electroactive, mechanical, and structural properties. The electrical charges generated via piezoelectric effects stimulate essential cellular functions in biological systems, such as adhesion, proliferation, and differentiation, and promote the immediate regeneration of complex tissues in bone and neural systems. PVDF has been successfully utilized in artificial organs, including artificial hearts, kidneys, and blood pumps [7,18,19], thanks to its durability, biocompatibility, and chemical stability in demanding physiological environments. Its piezoelectric behavior facilitates electrical transport and activation of biological responses in implanted systems. Moreover, PVDF can be processed into fibrous and porous bulk structures that support

cellular growth and guide tissue formation, enabling scaffolds to replicate the architecture of the regenerated target tissue [7,11–24].

Cell membranes can store electrical charges and participate in many cellular interaction processes, which are studied by changes in the membrane potential. Impedance analysis provides valuable insight into the surface response that influences membrane morphology and functionality. Most vertebrate cells exhibit limited proliferative potential due to telomere shortening, a process known as cell senescence. Telomerase, the enzyme responsible for maintaining telomere integrity, is inactive in most somatic cells, resulting in progressive telomere degradation with each division. Despite these limitations, biomaterials in contact with biological fluids or tissues can influence a wide range of cellular responses, collectively defining their "biocompatibility." This term encompasses all interactions between materials and cells. Among such materials are synthetic polymers, including polyethylene, polyvinyl, polyamide, polysulfone, and polyvinyl difluoride (PVDF) [3,6,8,25].

Finally, electrospinning remains a novel technology for producing nanofibrous mats with high surface-to-volume ratios and ECM-like structures. This approach has gained significant attention in tissue engineering due to its ability to produce nano- and microscale fibers that enhance cell adhesion, proliferation, and differentiation. The process involves applying a high-voltage electric field to a polymer solution, which results in the formation of solidified fibers. Its adaptability makes it ideal for fabricating functional scaffolds for biomedical use, particularly in tissue engineering. In this study, Hep-G2 cells were cultured using EMEM (Eagle's Minimum Essential Medium), which was supplemented with 10% fetal bovine serum. A piezoelectric PVDF polymer was chosen as a scaffold for culturing Hep-G2 cells due to its relevance in replicating both healthy and pathological tissue behavior. Studying 3D scaffold environments provides valuable insights into the evolution of natural tissues and offers a promising platform for testing regenerative treatments, such as skin repair therapies. This research aims to evaluate the biocompatibility behavior of electrospun PVDF polymer membranes in cell culture using the electrochemical impedance spectroscopy (EIS) technique, focusing on cell growth and behavior of Hep-G2 cells deposited on the fabricated PVDF mat.

This work also contributes to the growing field of piezoelectric biomaterials by providing a comparative perspective on the performance and applicability of the developed scaffold to existing materials, such as PZT and PVDF-TrFE. PZT exhibits strong piezoelectric properties; however, it is not recommended due to its high toxicity resulting from lead content. The proposed scaffold prioritizes biocompatibility and biodegradability, aligning with the biomedical requirements noted by Li et al. (2019) and Bai et al. (2021) [26,27]. In contrast to PVDF-TrFE, which has been widely studied for its flexibility and processability, electrospun PVDF material exhibits an enhanced piezoelectric response and improved surface properties that favor cellular adhesion and proliferation [27]. Furthermore, in contrast to traditional non-piezoelectric scaffolds that function passively by providing only mechanical support, this new scaffold actively generates localized electric stimuli in response to physiological movements. This electromechanical interaction significantly promotes tissue regeneration and cell differentiation, which has been demonstrated as an advantage of piezoelectric scaffolds in regenerative medicine [25,28,29]. Therefore, the scaffold presented in this study stands out as a multifunctional and safer alternative that links the gap between bioactivity, electrical functionality, and structural support.

2. Materials and Methods

This study investigates the behavior of a specific cell line (Hep-G2, a human liver carcinoma cell line) that typically resides in native tissues and is exposed to non-homogeneous media conditions. However, the Hep-G2 cell line was intentionally selected as a primary

biological cell model due to its robust adhesion capacity, high proliferation rate, and well-characterized response in vitro, which makes it suitable for assessing biocompatibility and cell–material interactions of the PVDF membranes. The cells were cultured on a polyvinylidene difluoride (PVDF) mat consisting of randomly oriented nanofibers, which replicates the structural complexity of the extracellular matrix. This fibrous substrate is specifically designed to mimic the irregular and multidirectional arrangement of ECM architecture, which is an essential factor for promoting cell adhesion, proliferation, and functional activity within dynamic biological environments. In this context, electrospinning has emerged as a leading technique for producing polymeric nanofiber membranes. Its simplicity, adaptability, and capacity for precise control over process parameters during membrane fabrication make electrospinning particularly well suited for developing biomedical scaffolds in tissue engineering, providing a promising tool for applications in regenerative medicine.

The polyvinylidene difluoride $(C_2H_2F_2)_n$ polymer used in powder form in this study was purchased from Sigma-Aldrich (Burlington, Massachusetts, USA) (CAS No. 24937-79-9), with a molecular weight of approximately 534,000 g/mol and density of 1.74 g/mL at 25 °C. The dimethylformamide (DMF, CAS No. 68-12-2) and acetone (CAS No. 67-64-1) solvents used for polymer dissolution were also purchased from Sigma-Aldrich (Burlington, Massachusetts, USA), analytical reagent grade. The Hep-G2 cell line (ATCC® HB-8065™) was obtained from the American Type Culture Collection (ATCC) (Manassas, Virginia, USA) and cultured following the supplier's recommended protocol using DMEM supplemented with 10% fetal bovine serum (FBS) and 1% penicillin-streptomycin.

2.1. Design of PVDF Fiber Mats

The fiber mats investigated in this study are predominantly composed of polyvinylidene difluoride (PVDF), a chemically inert electroactive polymer. These PVDF polymeric membranes were produced through the electrospinning technique with a custom-built laboratory apparatus, as illustrated in Figure 1. This apparatus is equipped with a DC power supply capable of delivering voltages ranging from 0 to 25 kV, which generates the high-voltage electric field required to induce electrostatic forces that draw the polymer solution into ultrafine fibers [30]. In this particular case, a voltage of 15 kV is applied to achieve the desired polymer deposition on the aluminum substrate by electrospinning. As denoted in Figure 1a, the positive DC terminal (anode) is connected to a syringe filled with a 3 cm^3 volume of reservoir and a hypodermic needle (0.8 mm × 40 mm), which delivers the polymeric solution. The negative terminal (cathode) is attached to a grounded collector substrate. In this configuration, the syringe acts as the anode, generating a continuous jet of polymer solution directed toward the collector substrate. The collector consists of an aluminum foil sheet mounted on a copper plate, serving as a conductive cathode electrode and providing a suitable surface for fiber deposition. The collector, measuring 10 cm × 15 cm, acts as the charged substrate onto which the electrospun fibers accumulate, as shown in Figure 1b.

The precursor reagent was prepared by dissolving 10 pellets of PVDF, each weighing 0.06 g, in 2.4 g of solvent (N, N-dimethylformamide-DMF $(CH_3)_2N$-CHO) to achieve a polymer concentration of 20% (*w*/*w*). The mixture reagent was heated at 110 °C for 1.5 h prior to electrospinning to ensure complete dissolution and homogeneity. During the electrospinning process, the distance between the needle tip and the collector substrate was 9 cm. After deposition, the electrospun PVDF membranes underwent a post-treatment heat process at 100 °C for 24 h to improve polymer crystallinity. The membrane thickness and pore size were controlled by adjusting the electrospinning time, enabling the creation of tailored membrane structures. Consistent with findings reported in the literature [6,8], the resulting membranes predominantly exhibited the characteristic β-phase, which is

favorable for electroactive applications. The fabricated membranes typically presented a thickness ranging from 90 to 100 nm and an elliptical shape deposition profile, with a major axis measuring approximately 9 cm and a minor axis of 7.5 cm. The fiber diameters were distributed within a range of 50 to 700 nm, reflecting the influence of the electrospinning parameters on fiber formation.

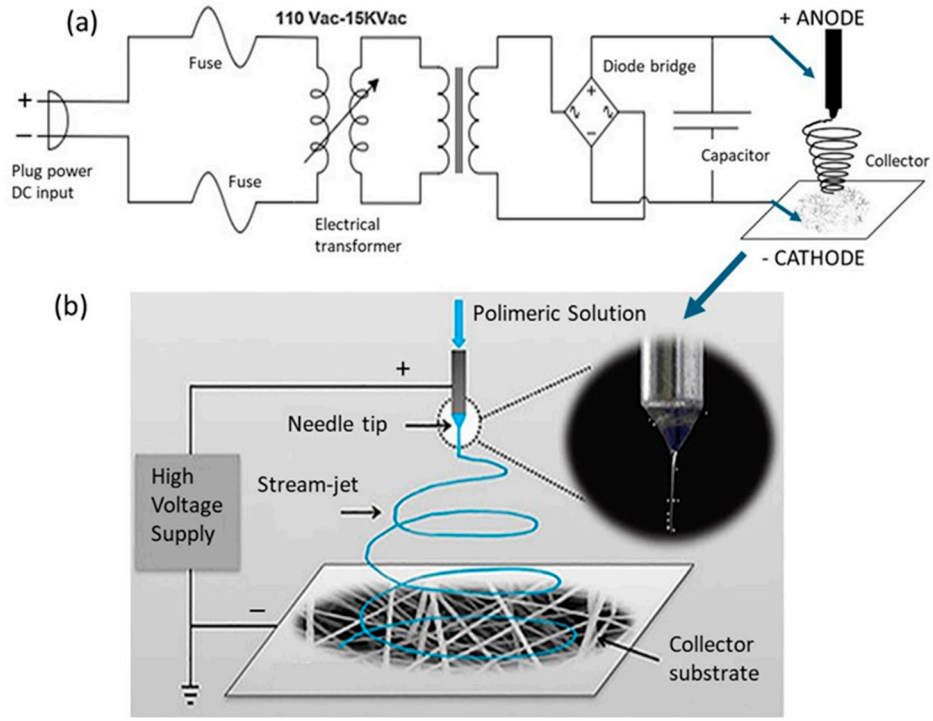

Figure 1. Schematic illustration of the electrospinning system setup, depicting (**a**) the electrical circuit configuration used for high-voltage conversion and (**b**) the polymer ejection mechanism driven by the applied electric field through electrode connections [30].

2.2. Cell Culture

The methodology for the Hep-G2 cell culture involves carefully preparing sterile laboratory environment and maintaining optimal conditions to support cell growth. For the experimental procedure aimed at promoting the growth of hepatocellular carcinoma Hep-G2 cells, a 0.5 cm^2 sample was obtained from the electrospun PVDF membrane, which had been previously prepared, as described in Section 2.1. The PVDF membrane and all cell culture equipment were sterilized inside a laminar flow cabinet using ultraviolet (UV) light exposure for 2 h to ensure aseptic conditions. The Hep-G2 cells were cultured under suitable conditions using Dulbecco's Modified Eagle Medium (DMEM), enriched with elevated concentrations of amino acids and vitamins, supplemented with 10% fetal bovine serum (FBS), and fortified with antibiotics to prevent contamination. A quantity of 500 µL of Trypsin-EDTA solution was added to the cultures for 5 min to facilitate cell detachment and prevent agglutination. Experimental cultivation was conducted in T-flask containers with surface areas ranging from 25 to 175 cm^2, containing 6–8 mL of culture medium per flask. Typically, the cells grow to approximately 1×10^7 adherent cells and 1×10^8 cells in suspension, providing a practical scale for space in an incubator and performing repeated passages necessary for cultivation [31]. A 0.5 cm^2 section of the electrospun PVDF fiber mat was used for scaffold evaluation, and the experiment was organized into three groups. The first group involved culturing cells on a glass substrate in direct contact with the fiber mat, the second used a cell-adherent plastic container with the PVDF fiber mat, and the third served as a control, cultured solely in a plastic container

without the fiber mat. This arrangement was designed to assess cell adhesion behavior on PVDF fibers within two different environments: glass and cell-adherent plastic. All cultures were incubated under standard conditions at 37 °C, with 95% humidity and 5% CO_2, to ensure proper physiological conditions [32]. Cell adhesion and proliferation were periodically monitored using an inverted phase-contrast microscope (Olympus IX-71, Nagano, Japan) to evaluate confluence, morphology, and cell adhesion to the substrate.

2.3. Cell Growth Control and Viability

According to the literature [27], cell growth and viability were monitored using an inverted microscope equipped with a 10× magnification objective lens, tracking the development of the cell culture over four days. Three distinct culture setups were prepared to evaluate cell behavior under three different substrate conditions. A quantity of 200 µL of Methylene Blue was applied to each sample for 1–3 min to facilitate cell visualization. The first culture (C1) was placed in a glass T-flask with a PVDF fiber mat. Since cells typically exhibit poor adhesion to the glass surface, this condition allowed for the assessment of cell attachment exclusively to the fiber surface. The second culture (C2) involved a plastic T-flask containing a PVDF fiber mat, which allows for the evaluation of cellular proliferation on the polymeric fibrous surface in a favorable adhesion environment. The third cell culture (C3), which served as the control, utilized a plastic T-flask without any additional substrate. In this condition, cells were expected to naturally adhere directly to the native plastic surface of the flask. These three conditions (C1, C2, and C3) were strategically designed to confirm the cellular growth on the PVDF fiber mat and to isolate the effects of the flask substrate material. As shown in Figure 2, this comparative analysis enables a more precise interpretation of cell–material interactions. After the staining process, any excess of Methylene Blue was carefully removed from each sample by repeated rinsing with distilled water to prevent interference during microscopic analysis.

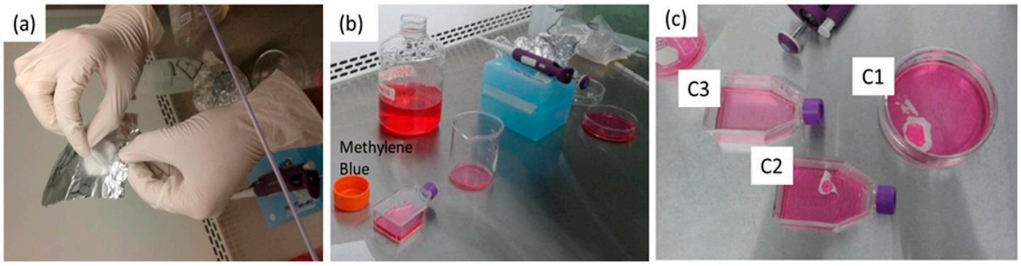

Figure 2. Experimental setup process for preparing and staining Hep-G2 cell culture. (**a**) Careful handling of a PVDF membrane under a biosafety cabinet to ensure a contamination-free environment; (**b**) essential materials and instruments required for the experiments; (**c**) schematic representation of the three distinct cell experimental conditions (C1—cells cultured on a PVDF fiber mat placed inside a glass T-flask); (C2—cells cultured on a PVDF fiber mat placed in a plastic T-flask); and (C3—cells grown directly in a plastic T-flask as the control group).

2.4. Characterization of Hep-G2 Cells Cultivated on PVDF Fiber Mats

2.4.1. Scanning Electron Microscopy and Elemental Composition Analysis

The morphology and microstructure of the electrospun fiber mats were characterized using a scanning electron microscope (SEM, JXA-8200, JEOL, Tokyo, Japan), which was employed to capture high-resolution surface images. The SEM was operated at an accelerating voltage of 15 keV to optimize image contrast and resolution of the surface topography analysis. Prior to imaging, the samples were sputter-coated with a thin layer of gold to enhance surface conductivity and minimize charging effects during electron beam exposure. Additionally, elemental distribution on the fiber mats was examined using an energy-dispersive X-ray spectroscopy (EDS) technique coupled to the SEM. EDS analysis

provided semi-quantitative information about the elemental composition of the fiber mats. The resulting spectra allowed the identification of the primary chemical elements present in the fibers, contributing to a comprehensive assessment of the material's structural and compositional integrity.

2.4.2. Electrochemical Impedance Spectroscopy Analysis

Electrochemical tests of PVDF fiber mats with cultivated Hep-G2 cells supported as described in the experimental C2 condition were conducted in a physiological environment, using a 0.9% sodium chloride (NaCl) saline solution, which is commonly used in biomedical applications to restore electrolyte salts lost through dehydration. Squared samples of the C2 fiber mats with cells deposited were analyzed in an electrochemical cell design, as shown in Figure 3. A conventional three-electrode configuration was used [33–35]; at the top of the cell, an Ag/AgCl reference electrode (RE) was connected in parallel with a platinum wire, which was connected in series to a 33 μF/10 mV capacitor element. This arrangement mitigates signal distortion caused by high-frequency interference, a prevalent problem in piezoelectric materials. The counter electrode (CE) consisted of a graphite bar, whereas, at the bottom of this cell, the test sample (electrospun PVDF fiber mat) acted as the working electrode (WE) with an exposed active surface area of 0.8 cm^2 to the electrolyte solution. Electrochemical measurements were performed using a PARSTAT-4000 potentiostat/galvanostat (Princeton Applied Research, Oak Ridge, TN, USA), which was connected to a computer and controlled by VersaStudio software (v.6) for data acquisition. The experimental sequence began with an open-circuit potential (OCP) monitoring for 10,000 s, allowing the system to reach a thermodynamic equilibrium state without applying a current pulse. Subsequently, an alternating current (AC) signal with a small amplitude was used as a perturbation signal to conduct electrochemical impedance spectroscopy (EIS). The EIS measurements were carried out over a frequency range from 10^6 to 10^{-3} Hz, with a 10 mV signal amplitude and 10 data points recorded per decade. The resulting impedance data obtained were represented as Nyquist plots (Zreal vs. −Zimag), and analyzed through fitting with various equivalent electrical circuit (EEC) models. A total of five distinct EEC models were proposed to better explain the electrochemical behavior of the system. Measurements were performed after immersion periods of 5, 24, 72, 120, and 168 h to monitor time-dependent changes in electrochemical performance.

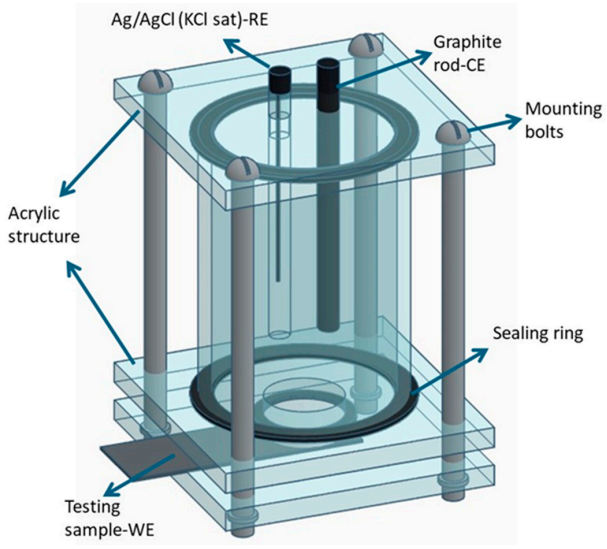

Figure 3. Schematic representation of the three-electrode electrochemical cell configuration, designed explicitly for EIS testing of electrospun PVDF fiber mats under physiological conditions (NaCl 0.9%) [33–35].

3. Results and Discussion

3.1. Cell Culture Dynamics on Different Substrate Materials

Figure 4 shows the results obtained from cell culture experiments conducted on various substrates, including an electrospun PVDF fiber mat. The images illustrate the behavior of Hep-G2 cells in terms of adhesion, spatial distribution, and morphology after four days of incubation under DMEM culture conditions. Additionally, Figure 4a displays the structure of the PVDF membrane before cell culture, exhibiting visible spherical aggregates of polymeric fibers integrated into a continuous, thin film that grows uniformly on the entire surface of the metallic substrate. The cells assumed a notably lower adhesion density when cultured on a glass substrate (test condition C1), as depicted in Figure 4b. The smooth and rigid surface of glass typically results in unfavorable cell adhesion. In contrast, Figure 4c provides a macroscopic view of the PVDF fiber mat used in test condition C2. The mat exhibits a porous, fibrous structure composed of thin and flexible polymeric fibers. This fibrous and porous architecture promotes better cell adhesion and even uniform distribution. Hep-G2 cells appeared to grow along the fibers, closely mimicking the natural extracellular environment matrix (ECM). This behavior supports better adhesion and the potential for enhanced cell differentiation. In the control condition (C3-Figure 4d), where cells were cultured on a standard plastic T-flask substrate, cells appeared randomly scattered and exhibited an epithelial-like morphology. Certain regions displayed more intense staining in groups, suggesting localized zones of strong adhesion and homogeneous cellular growth. These observations highlight the significant impact of substrate material on cellular behavior, demonstrating that electrospun PVDF fiber mats provide a favorable environment for Hep-G2 cell growth. This supports their potential application as scaffolds in biological and biomedical research.

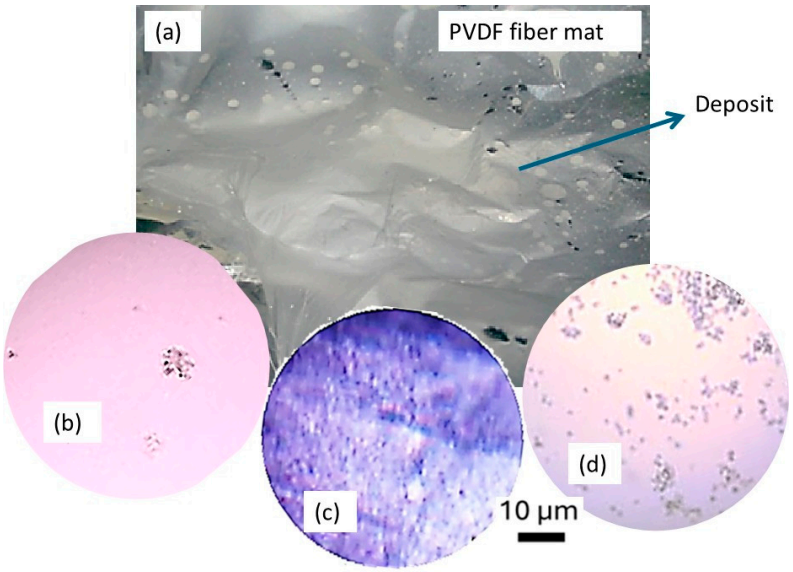

Figure 4. Optical microscopy images captured at 10X for a Hep-G2 cell culture under different conditions: (**a**) non-cell culture on PVD-fiber mat, (**b**) Hep-G2 cell supported on PVDF membrane with glass, (**c**) Hep-G2 cells on a PVDF membrane supported by a plastic, and (**d**) Hep-G2 cell culture with a plastic support as a control.

The better adhesion of Hep-G2 cells on the plastic substrate compared to the glass is mainly due to differences in surface properties. Plastic surfaces often exhibit a slightly hydrophilic nature and a microscopically rougher texture, which promotes better protein adsorption from the culture medium, a critical step for cell attachment. The adsorbed proteins provide attachment sites for nucleation on the cell membrane, facilitating adhesion

and subsequent cell spreading. In contrast, the glass surface is typically smoother and more hydrophobic, which limits protein adsorption and consequently reduces the number of adhesion sites for cells. This observation is supported by the experimental results shown in Figure 4b, which indicate a lower concentration of attached protein groups, resulting in reduced cell adhesion on glass substrates. The PVDF fiber mat provides an even more favorable environment by mimicking the natural extracellular matrix (ECM) due to its fibrous and porous structure. It offers a high density of attachment points that enhance cell distribution and growth, thereby supporting improved cell–matrix interactions.

3.2. Control and Growth of Hep-G2 Cells

Based on the favorable results observed with the plastic substrate, Figure 5 presents optical microscopy images of Hep-G2 cells cultured after four days of incubation under standard DMEM conditions. Each image captures the cellular morphology and distribution at different magnifications for the most favorable growth environment, which was for the C2 condition. The cells exhibit well-defined morphology, are densely distributed, and proliferate across the observed area. The absence of contamination, high confluence, and strong adhesion to the substrate also characterize them. This optimal cellular behavior can be attributed to the plastic surface's physicochemical properties, which efficiently support cellular adhesion and proliferation. The growth kinetics of Hep-G2 cells on the plastic substrate follows a well-defined progression. Within the first 24 h, cells adhere and begin spreading across the substrate surface. By the second day, cells enter an exponential growth phase, marked by rapid cell division and the formation of dense cellular clusters. The plastic's relatively developed hydrophilic surface nature and suitable surface texture promote enhanced interaction between the cells and substrate, facilitating uniform distribution while minimizing segregation. By the fourth day, the culture reaches a high confluence rate, forming a consistent monolayer indicative of strong substrate adhesion and effective nutrient absorption from the DMEM medium. These results highlight the synergistic role of favorable substrate properties and a nutrient-rich culture medium, DMEM, in supporting cell viability, sustained proliferation, and maintaining the characteristic epithelial-like morphology of Hep-G2 cells.

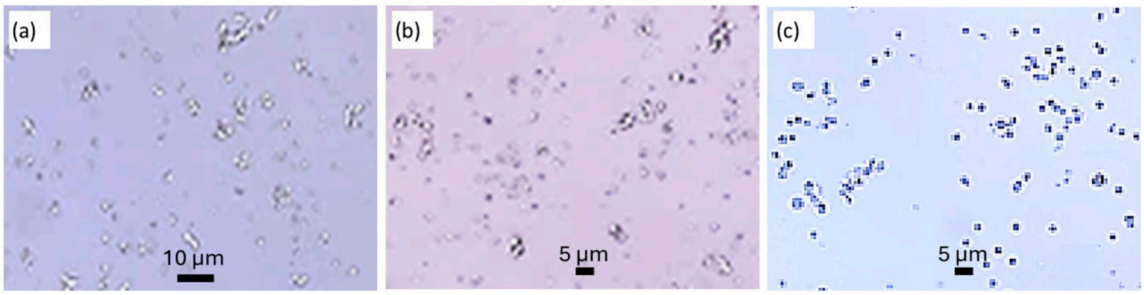

Figure 5. Optical microscopy images were captured at 10X and 20X magnifications for a Hep-G2 cell culture with plastic support as a control. The images highlight cellular morphology (**a**), adhesion (**b**), and confluence (**c**) after four days of incubation under DMEM conditions.

3.3. Membrane Staining with Methylene Blue

After staining the membranes with Methylene Blue reagent, it was observed that Hep-G2 cells successfully adhered to and proliferated on the PVDF membrane fabricated by electrospinning technology. The staining process allowed for enhanced visualization of cell distribution and morphology, confirming effective cell attachment and growth. General microscopy analysis of the membrane (test condition C2) is shown in Figure 6, where images were captured at magnifications of 10×, 40×, and 60×, clearly demonstrating the formation of confluence cell groups adhered firmly to the PVDF membrane. The analysis of Figure 6a

revealed a uniform staining pattern, indicative of homogeneous cell layer formation. At the same time, variations in color intensity suggested localized differences in cell density across the polymer membrane. Additionally, the presence of circular morphology may correspond to cellular debris resulting from the staining procedure. These findings confirm that the PVDF membrane provides a suitable environment for Hep-G2 cell adhesion and proliferation, thus demonstrating its possible use as a scaffold for cell culture applications.

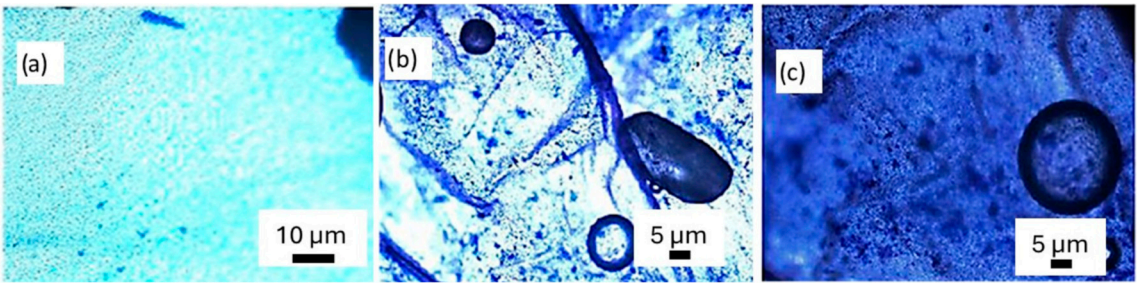

Figure 6. Optical microscopy analysis of the PVDF membrane at (**a**) 10×, (**b**) 40×, and (**c**) 60× magnifications, showing Hep-G2 cell adhesion, distribution, morphology, and structural integrity.

The structural analysis of the fiber mats suggested that the resulting membranes predominantly consisted of the electroactive polar β-phase, which is favored by the combination of the polymer's intrinsic dipolar nature and the high-voltage conditions applied during the electrospinning process [12,13]. This β-phase is known to be the most electroactive, and it is characterized by a polar crystalline configuration that develops a considerable electric dipole moment in a single direction, imparting a significant piezoelectric effect to the membranes. The presence of the β-phase facilitates the alignment of dipoles in the polymer chains, particularly when exposed to a strong electric field. This alignment contributes to enhanced electrostatic interactions, increased surface charge density, and improved hydrophilicity. These factors collectively promote protein adsorption, which is essential for cell adhesion and proliferation, principally for Hep-G2 cells.

In Figure 6b,c, microscopy images reveal the structure of cell nuclei in an elliptical and circular shape within the fibrous structure, with measured major and minor radii of approximately 19 µm and 7.5 µm, respectively. These features correspond to vesicle-like particles adherent to Hep-G2 cells, indicating effective cell attachment. Additionally, Figure 6a shows a highly nano-porous structure and the rough surface texture appearance of the fiber mat with the cell culture. Such porosity and surface roughness are advantageous in fiber mats and are desirable effects in scaffolds because they promote cell culture adherence to the scaffold. However, the combination with the β-phase provides enhanced bioactivity, a characteristic that supports cell adhesion, differentiation, and proliferation. Furthermore, the piezoelectric response of PVDF membranes promises to be used in electrically stimulated tissue regeneration, mimicking the native bioelectrical signals present in biological tissues.

3.4. Scanning Electron Microscopy (SEM) Analysis

Figure 7 presents two representative micrographs obtained by scanning electron microscopy (SEM) at magnifications of 750× and 1500×, illustrating the morphology of Hep-G2 cells cultured on an electrospun PVDF fiber mat (substrate). A high density of cells is observed, growing heterogeneously and distributed well across the entire substrate surface, and showing predominantly spherical morphology. This suggests that during the electrospinning process, the fibers tend to agglomerate due to electrostatic interactions, insufficient solvent evaporation, and surface tension forces. At 750× magnification, several cells interact with the polymer's underlying fibers. A closer view of the cells at 1500×

magnification reveals their preferential adhesion sites and distinct cell–fiber interactions. The observed variability in cell size and shape is significant, which is critical for understanding cell–material interactions, as the presence of a fibrous structure may guide cell attachment and orientation, making an ideal scaffold suitable for biomedical applications. As shown in Figure 7a, the PVDF fibers range in diameter from approximately 50 to 700 nm and are randomly oriented. As seen in Figure 7b, Hep-G2 cells successfully adhered to these fibers, suggesting that the topographical and morphological characteristics of the mat play a crucial role in promoting effective cell–substrate interactions.

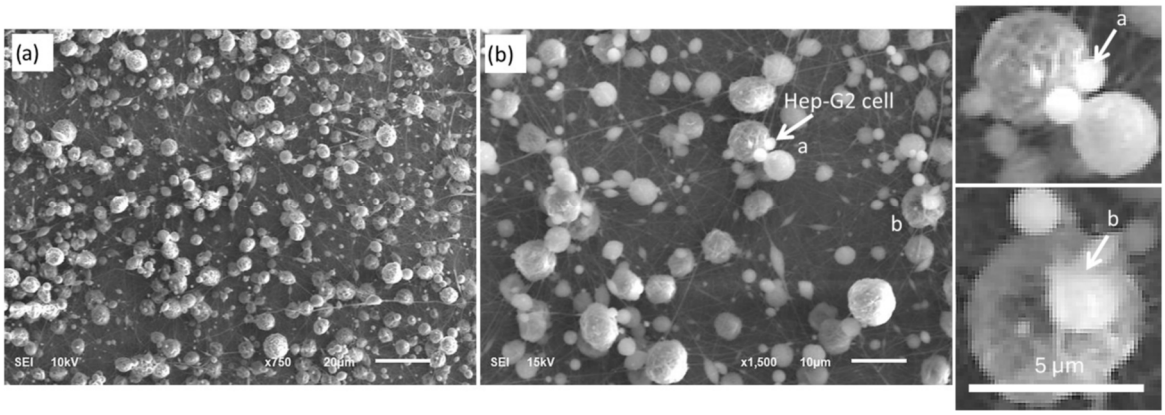

Figure 7. High-resolution SEM images of the electrospun PVDF fiber-mat, illustrating surface morphology and structural characteristics at different magnifications: (**a**) 750× and (**b**) 1500×. The images highlight the fiber distribution and cell–substrate interactions relevant to Hep-G2 cell culture.

3.5. Energy-Dispersive X-Ray Spectroscopy (EDS) Analysis

Hep-G2 cell culture on the PVDF membrane was further analyzed using the Energy Dispersive X-ray Spectroscopy (EDS) technique. Figure 8 displays a view of the PVDF membrane at a 2200× magnification, where a green cross mark indicates the specific EDS analysis on a selected spherical fiber. The corresponding EDS spectrum is shown in Figure 8, and the elemental composition results are summarized in Table 2. The EDS analysis revealed the presence of important elements associated with the polymeric fiber mat and biological matter, including carbon (C), fluorine (F), oxygen (O), phosphorus (P), sodium (Na), magnesium (Mg), and chloride (Cl). The presence of biologically relevant elements (O, P, Na, Mg, and Cl) suggests successful cell adhesion and interaction with the PDVF polymer scaffold. Meanwhile, the prominent fluorine signal confirms the presence of PVDF on the membranes deposited by electrospinning, validating its function as the principal component of the scaffold material.

- Carbon (C) and fluorine (F): These elements are characteristic of the PVDF polymer, confirming the integrity and presence of the polymer matrix.
- Oxygen (O), phosphorus (P), and sulfur (S): Probable chemical elements derived from cellular components such as phospholipids, proteins, and nucleic acids or potentially from surface modifications introduced during processing.
- Sodium (Na) and chlorine (Cl): These elements may originate from residual components of the cell culture medium.
- Silicon (Si): Element possibly associated with metal-based coatings applied to enhance the bioactivity of the membrane.
- Aluminum (Al): Signal detected from the aluminum foil substrate (Al-foil) that supports the PVDF membrane.

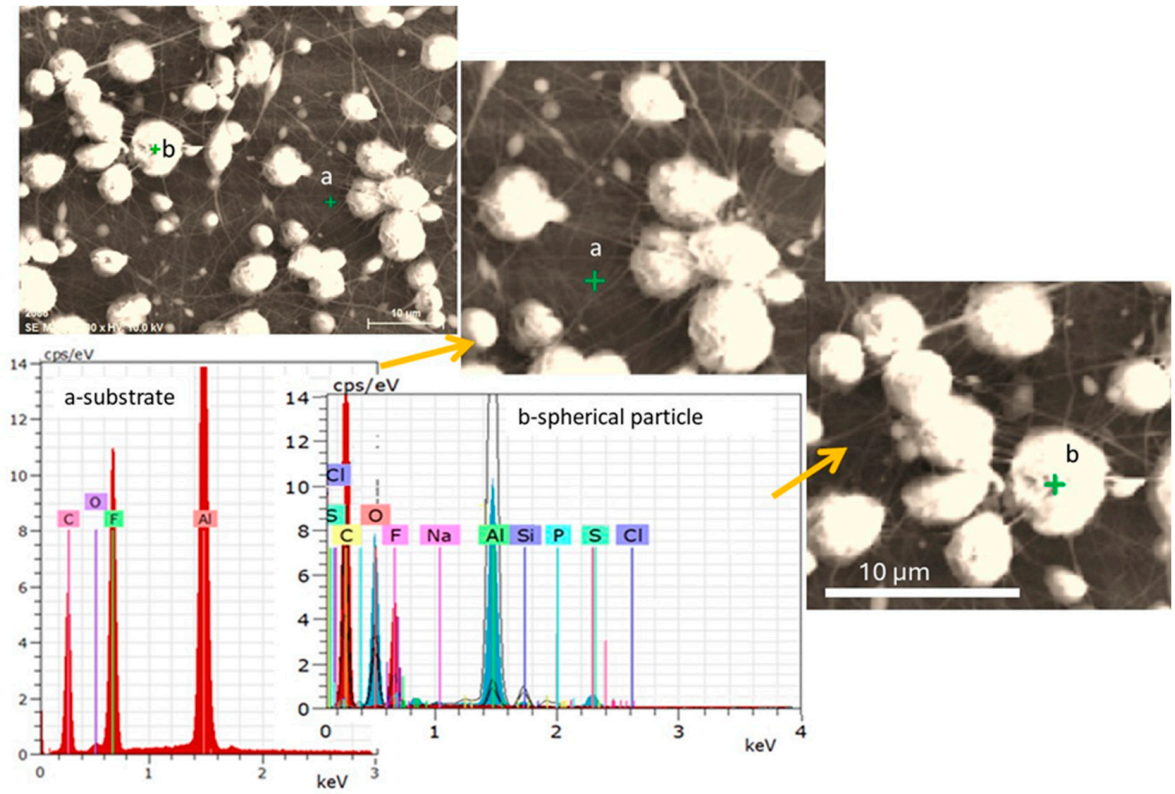

Figure 8. SEM micrograph and corresponding EDS analysis of the PVDF membrane. The green marker indicates the location of the EDS analysis. Point "a" corresponds to the EDS spectra obtained from the aluminum foil substrate, while point "b" represents the EDS spectra of a spherical particle observed on the PVDF membrane.

Table 2. EDS results show the elemental analysis in terms of mass percentage and the dispersal of energy in keV.

Location Region of EDS	Elemental Composition in Mass %								
	C Carbon	O Oxygen	F Fluorine	Al Aluminum	S Sulfur	Cl Chlorine	P Phosphorus	Si Silicon	Na Sodium
Energy-Kev	~0.28	~0.52	~0.68	~1.49	~2.31	~2.62	~2.02	~1.74	~1.04
a	35.98	1.29	33.87	28.85	—	—	—	—	—
b	57.23	27.45	13.08	—	1.6	0.43	0.10	0.06	0.05

a PDVF membrane substrate. b Spherical fiber particle.

The SEM images provide information about the distribution and morphological characteristics of the cultured Hep-G2 cells. At the same time, the EDS spectra confirm the biologically relevant elements associated with cellular adhesion and proliferation on the polymeric PVDF scaffold. These findings support the potential use of electrospun PVDF membranes in biomedical scaffolds for liver tissue engineering and regenerative medicine. Moreover, their application could be extended to restoring damaged tissues in severe skin wounds or burns, where nanofibrous polymeric films can facilitate healing and tissue regeneration.

3.6. Electrochemical Impedance Spectroscopy Analysis; Application

3.6.1. Electrical Circuit Model Analysis

In this study, EIS was employed to evaluate the biocompatibility of PVDF membranes used as support mats for Hep-G2 cell growth and structural regeneration. The measurements were conducted in a physiological electrolyte solution (NaCl 0.9%), which maintains a pH between 7.0 and 7.4. This solution simulates the ionic composition of biological

fluids, providing a conductive and controlled environment that mimics in vitro conditions for cellular metabolism. Impedance variations were monitored over time to assess cell adhesion, proliferation, and surface modifications induced by cellular activity on the PVDF membrane. The EIS data obtained are shown in the form of Nyquist and Bode plots, which represent the transient response of the electrochemical system. This behavior can be described using an equivalent electrical circuit (ECC) model, which allows for the characterization of surface electrochemical changes associated with the presence and development of the cell film on the PVDF substrate.

In this study, four different ECC models were proposed to analyze the behavior of the EIS data obtained after exposing the PVDF fiber mat at different times in the electrolyte test solution. These models are based on combinations of resistors (R) and capacitors (C) arranged in series and parallel configurations, as described below. The simplest model (Figure 9a) represents a basic Randles-type circuit comprising a single resistor and capacitor in parallel, which is suitable for describing systems with minimal interfacial complexity. In contrast, the more advanced models (Figure 9b–d) incorporate multiple RC units, indicating the presence of several electrochemical relaxation processes occurring at different depths of the electrode interface. These additional elements are necessary to represent the more complex behavior of the system, such as the interaction between cells and the PVDF substrate. All proposed models include the solution resistance (R_s), which accounts for the ionic conductivity of the electrolyte. The capacitance of the cell layer (C_c) represents the dielectric response of the PVDF cell interface, while the corresponding resistance (R_c) simulates ionic transport through the cell layer, both of which collectively define the total impedance of the biological cell layer.

Furthermore, the charge transfer resistance (R_{ct}) and the double-layer capacitance (C_{dl}) are introduced to characterize the electrochemical interactions at the cell–substrate interface. R_{ct} quantifies the resistance to electron transfer across the electrode–cell interface, and C_{dl} reflects the capacity of the electrical charge storage at the interface due to the formation of an electric double layer. These parameters provide valuable insights into the surface reactions and bioelectrochemical behavior of PVDF scaffolds that support the growth of Hep-G2 cells.

Model R(CR). Figure 9a depicts the simplest equivalent electrical circuit (ECC), consisting of a capacitor (C_{dl}) connected in parallel with a resistor (R_{ct}) and then connected in series with another resistor element (R_s). This configuration represents two impedance components (Z_1 and Z_2). Equation (1) describes the total impedance, which governs the behavior of the kinetic reaction at a frequency-dependent system and is derived from the R(CR) circuit model, where R_s denotes the electrolyte resistance in Ω (accounting for the ionic conductivity of the electrolyte), R_{ct} models the charge transfer resistance (Ω), associated with the kinetics control of electron transfer at the electrode–electrolyte interface, C_{dl} is the double-layer capacitance (F), resulting from the capacitance formed due to the charge separation at the electrode–electrolyte interface. Z_1 refers to the interfacial impedance, and Z_2 is the total impedance of the system that describes the kinetics of the electrochemical reaction at the interface. $j = \sqrt{-1}$ is the imaginary unit and ω is the angular frequency of the applied AC signal $\omega = 2\pi f$, where f is in Hz. This circuit provides valuable information related to the electrochemical response of the biomaterial PVDF membrane during Hep-G2 cell culture. It also monitors the changes in interfacial capacitance, which can be attributed to protein adsorption and cell attachment. This circuit was also used to study cell adhesion on biomaterials and could indicate variations in the capacitance charge of electrons at the interface due to the adsorption of a group of cell attachments on the fiber mat.

ELECTRICAL MODEL DESIGN	EQUATION	MECHANISM OF STUDY
(a) 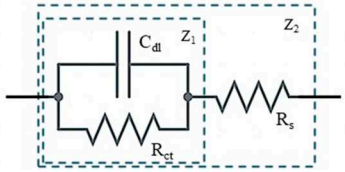	(1)	• Corrosion reaction. • Protective coatings. • Biosensor, batteries, and fuel cell analysis. • Electron charge transfer. • Double-layer capacitance
(b) 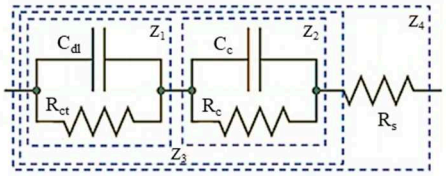	(2)	• Evaluation of protective (multilayer coatings). • Biosensors and tissue engineering studies. • Electrochemical response for biomaterials.
(c) 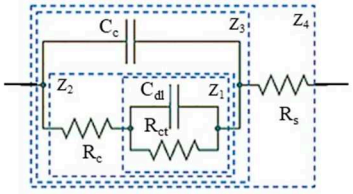	(3)	• Corrosion mechanism • Evaluation of protective coatings. • Biosensors application and energy storage.
(d) 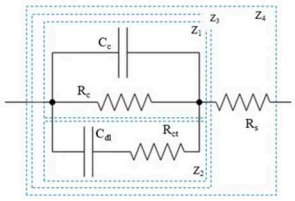	(4)	• Evaluation of protective coatings. • Biosensors application and energy storage. • Tissue engineering studies.

Figure 9. Comparative analysis of electrical equivalent circuit (EEC) models used to interpret the electrochemical impedance spectroscopy (EIS) data in biomaterial tested in 0.9% NaCl physiological solution. (**a**) R(CR) model, (**b**) R(CR)(CR) model, (**c**) R(C(R(RC))) model, and (**d**) R(RC(CR)).

$$Z_2 = R_s + \frac{R_{ct}}{1 + j\omega C_{dl} R_{ct}} \quad (1)$$

Model R(CR)(CR). Figure 9b shows an equivalent electrical circuit (ECC) model comprising the combination of two parallel resistors (R) and a capacitor (C) element connected in series. This configuration accounts for multiple impedance contributions labeled as Z_1 (PVDF interface), Z_2 (coating resistance), Z_3 (electrical capacitance), and Z_4 (solution resistance). The behavior of this multilayer system is mathematically described by Equation (2), which models the electrochemical interactions at different structural levels of the membrane and cell interface.

$$Z_4 = R_s + \frac{R_c}{1 + j\omega C_c R_c} + \frac{R_{ct}}{1 + j\omega C_{dl} R_{ct}} \quad (2)$$

Model R(C(R(RC))). As illustrated in Figure 9c, this ECC model is a more complex derivation, as described by Equation (3), with a pair of R and C networks connected in parallel. One pair includes the capacitor C_{dl} and resistor R_{ct}, which describe the electrochemical double-layer interface formed between the cell and the PVDF surface. The second pair consists of C_c and R_c, which are attributed to the properties of the PVDF coating. R_s is also included to account for the electrolyte resistance. This configuration

facilitates a more detailed interpretation of the interfacial and bulk properties of the scaffold PVDF membrane.

$$Z_4 = R_s + \frac{\left(R_c + \frac{R_{ct}}{1 + j\omega C_{dl} R_{ct}}\right)}{1 + j\omega C_c \left(R_c + \frac{R_{ct}}{1 + j\omega C_{dl} R_{ct}}\right)} \quad (3)$$

Meanwhile, the model R(RC(CR)) of Figure 9d is derived from the previous configurations and mathematically designed (Equation (4)) to describe the double-layer capacitance and the charge transfer resistance of the PVDF membrane immersed in the electrolyte. In addition, this circuit reflects the contribution of the dipole moment induced by the β-phase of PVDF, which enhances Hep-G2 cell proliferation. The presence of this electroactive phase influences the dielectric response of the system and modifies the scaffold's permittivity constant due to cell adhesion. This model can describe the biocompatibility and ion transport exchange at the membrane–cell interface, and also be used to study the cell adhesion and the biocompatibility of the biofilm with the system (scaffold–PVDF membrane) under test.

$$Z_4 = R_s + \frac{1}{\left(\frac{1}{R_{ct}} + j\omega C_c\right)} + \frac{1}{\left(\frac{1}{R_c} + j\omega C_{dl}\right)} \quad (4)$$

These electrical equivalent circuit (ECC) models are essential tools for analyzing the electrochemical behavior of complex systems, particularly in studying reaction mechanisms and biomaterial interactions. Each model represents a different level of electrochemical complexity, allowing the interpretation of charge transfer kinetics, capacitive behavior, and diffusion phenomena. The selection of an appropriate circuit model is determined by the structural and electrochemical characteristics of the system under study. For instance, simple circuits such as the one shown in Figure 9a are ideal for systems with single-layer coatings and relatively in contact with electrochemical interfaces, where the dominant parameters are charge transfer resistance and double-layer capacitance. In contrast, more sophisticated models illustrated in Figure 9b–d incorporate additional resistances and capacitances to simulate multilayered protective coatings, complex biomaterial interactions, and advanced physiological applications such as tissue engineering. These advanced circuit models offer a more realistic and detailed representation of electrochemical environments, which is particularly valuable for applications in tissue engineering and regenerative medicine. By more accurately modeling cellular adhesion, proliferation, and scaffold performance, they enhance the understanding of bioelectrochemical interfaces and contribute to the development of optimized biomaterials for clinical use.

3.6.2. Electrochemical Characterization Results

Figure 10 illustrates the electrochemical behavior of the polymeric surface at the open-circuit potential (OCP) as a function of the activation potential E (mV), measured in a 0.9% NaCl solution that simulates physiological saline conditions. The measurements were collected at five different immersion time intervals (5 h, 24 h, 72 h, 120 h, and 168 h) without an externally applied current signal, using an Ag/AgCl reference electrode. These OCP data provide information about the spontaneous electrochemical stability of the PVDF membrane over time. According to previous studies, Hep-G2 cells demonstrated favorable adhesion and proliferation when cultured on PVDF fiber mats, indicating that this polymer material provides optimal conditions for cellular growth and performance.

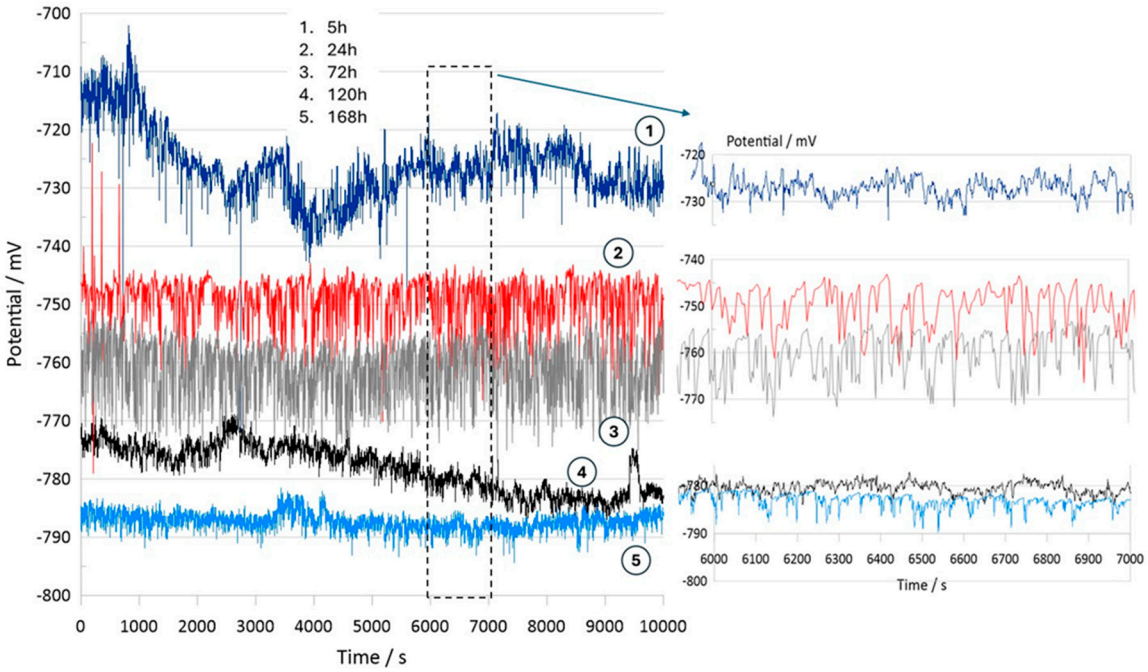

Figure 10. Open-circuit potential transients of the PVDF fiber mat with Hep-G2 cells, recorded over a continuous exposure period of 168 h in a 0.9% NaCl solution, simulating physiological conditions.

Consequently, Figure 10 presents the OCP curves for the PVDF fiber mat containing Hep-G2 cells that were cultured. The curve labeled 1 corresponds to the OCP transient after 5 h of immersion in a 0.9% NaCl solution. The curve displays significant signal fluctuations during the 10,000 s evaluation period, suggesting a stochastic electrochemical reaction process. These unstable potential variations, fluctuating between −710 and −730 mV, indicate an initial dynamic surface interaction. Notable changes in the potential value are observed, probably attributed to the ingress of chloride ions into the PVDF structure, which causes surface salt hydration and possibly activates the charge transfer mechanism. This behavior is likely influenced by ionic exchange mobility and adsorption at the interface, given the bioelectrical activity properties of the Hep-G2 cells, indicating their metabolic processes as mentioned in Table 3.

Specifically, hydroxide compounds progressively ingress into the polymeric structure. This observation suggests that the surface activation process is rapidly driven by ion transfer, which predominates during the initial hours of immersion in the system under study. This signal behavior is described by the following mathematical equation (Equation (5)):

$$V(t) = V_o e^{-t/\tau} + Asin(\omega + \varphi) + \eta(t) \quad (5)$$

where V_o is the initial transient voltage amplitude, τ expresses the characteristic time constant associated with the exponential decay of the signal, $Asin(\omega + \varphi)$ denotes the small amplitude oscillatory component as a function of angular frequency ω, and η(t) describes the random noise function imposed on the system response. The signal labeled number 1 exhibits periodic oscillations, which are modeled using the approximate signal based on a Fourier series, expressed as $\sum_{n=1}^{\infty} A_n cos(\eta\omega t + \varphi_n)$, where A_n represents the Fourier coefficients representing the amplitudes of the distinct frequency components that model the periodic oscillations, and φ_n represents the corresponding phase shifts. This mathematical approach effectively characterizes the complex oscillatory behavior observed during the early stages of surface activation and ion transport phenomena (Equation (6)),

where Fourier deconvolution is particularly effective in separating the intrinsic material response from external perturbation during the OCP measurements.

$$V(t) = \sum_{n=1}^{\infty} A_n cos(\eta\omega t + \varphi_n) + \eta(t) \quad (6)$$

Table 3. Description of open-circuit potential (OCP) transients for the PVDF fiber mat with Hep-G2 cells cultured after continuous exposure to a 0.9% NaCl physiological solution for 168 h.

Signal	Trasient Response	Characteristic
1		• Stochastic process. • Transient potential fluctuation. • Charge transfer process. • PVDF fiber mat interacting with Hep-G2 cells.
2–3	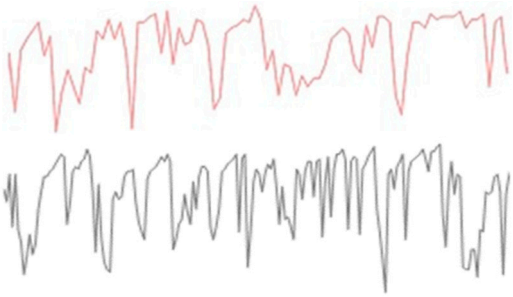	• Surface reactions on PVDF-based coating. • Capacitive charging/discharging effects. • Ion exchange and bioelectrical activity causing signal fluctuations. • Stochastic electrochemical reactions
4–5	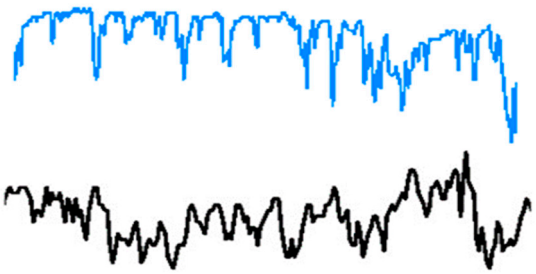	• Bioelectrical signals (ionic movement across the membrane). • Electron transfer mechanism by the ion adsorption process. • Cellular activity on PVDF membrane.

For immersion times of 24 h and 72 h (curves 2 and 3), the recorded signals exhibit pronounced higher-frequency fluctuations ranging from approximately −740 to −770 mV. This behavior suggests that the system could be influenced by perturbations associated with active electrochemical reactions like fast charge transfer kinetics and ion diffusion processes occurring on the PVDF membrane surface, indicative of capacitive charging effects. Additionally, certain sections of the signals display a possible periodicity pattern, which is further analyzed using the Fourier transform technique to identify and characterize the dominant frequency components that lead to the observed oscillatory behavior (Equation (7)).

$$V(t) = V_o e^{-t/\tau} + \sum_{n=1}^{\infty} A_n cos(\eta\omega t + \varphi_n) + \eta(t) \quad (7)$$

Stochastic electrochemical reactions suggest that the system undergoes continuous dynamic changes due to surface modifications and cellular activity. Ion exchange and bioelectrical processes contribute to signal fluctuations, reflecting the interactions between the PVDF membrane and the surrounding electrolyte. After 120 h (curve 4) and 168 h (curve 5) of immersion, a stable potential is observed, indicating that no significant changes on the surface were observed. The recorded signals appear to have small amplitude fluctuations with irregular downward peaks that suggest cell confluence and functional adaptation on the PVDF matrix, driven by cellular metabolic activity. This system maintains a relatively stable potential in the range of −770 to −790 mV. Over the extended immersion

period of 168 h, the OCP becomes progressively more stable, suggesting that the polymeric fiber mat undergoes no significant surface degradation under physiological conditions. Moreover, the increasingly negative shift in potential with immersion times indicates that the surface exhibits an active electron transfer mechanism, likely associated with the ion adsorption process. This facilitates surface activation and the formation of a dense, biocompatible monolayer film, indicative of a favorable biocompatibility response. These findings imply that the system reaches a steady state characterized by stable metabolic and electrical activity. This behavior is promising for biomedical applications, where the PVDF mat provides a suitable environment for Hep-G2 cell adhesion, proliferation, and cellular integration that will be in continuous interaction with body fluids. Therefore, this system demonstrates significant potential for applications in tissue engineering.

3.6.3. Electrochemical Impedance Spectroscopy (EIS)

The EIS displayed in Figure 11 are depicted as Nyquist and Bode plots, illustrating the ionic charge transfer and diffusion processes occurring at the PVDF material and electrolyte interface. The impedance measurements show two distinct time constants: the first, located at high frequency, is associated with surface-related phenomena, such as the presence of pores within the PVDF matrix; the second time constant corresponds to the charge transfer processes involving ions at the interface between the PVDF/Hep-G2 cell, the test sample, and the surrounding electrolyte. At 120 and 168 h of immersion, the EIS curves indicate a progressive charge transfer process occurring at the polymeric interface, beginning from the initial tests at 5 h and continuing up to 168 h of exposure in NaCl solution. A distinct time constant is observed at high frequencies and is associated with electrochemical phenomena occurring at the PVDF material–electrolyte interface. After 5 h of immersion, the system exhibits a semicircle arc with an amplitude of nearly 60 kΩ-cm^2, which subsequently decreases sharply to around 30 kΩ-cm^2 and eventually stabilizes at about 10 kΩ-cm^2. This behavior suggests that Cl^-, Na^+, and OH^- ions progressively pass through the polymeric matrix through its porous structure, as shown in curves 1, 2, 3, and 4. Simultaneously, the amplitude of a second time constant diminishes with increasing immersion time, leading to better consolidation of the porous surface by hydration products. This leads to a lower charge transfer resistance (R_{ct}), indicating less resistivity to electron flow compared to the initial value, thereby facilitating the accomplishment of the electrochemical reactions at the PVDF interface.

Pore hydration promotes the structural consolidation of the interface, enhancing the surface properties of the emerging biofilm and facilitating the transport of ionic species. Consequently, a change in the dielectric constant of the interface occurs due to pore hydration and imperfections in the developing biofilm. Nyquist plots typically exhibit a significant second semicircle at high frequencies, corresponding to the charge transfer resistance (R_{ct}) across the surface of the PVDF membrane. The diameter of these semicircles directly correlates with load transfer resistance; a larger diameter indicates greater stability of the material due to the formation of a hydrated biofilm. The Bode plots shown in Figure 11 further understand the mechanisms of charge transfer as a function of frequency, providing detailed information about the reaction kinetics and the processes controlling charge and mass transport. In this case, the magnitude of the absolute impedance ($|Z|$) and the phase angle (ϕ) of the sinusoidal signal applied to the interface are plotted throughout the measured frequency range.

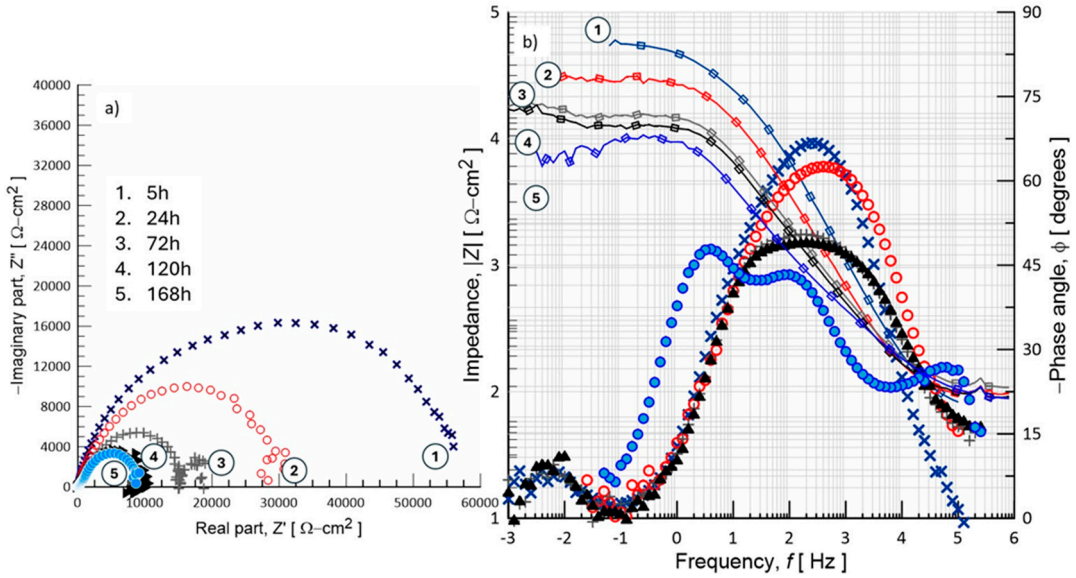

Figure 11. EIS response of the PVDF polymer/Hep-G2 cell samples during exposure to 0.9% NaCl solution, presented in (**a**) Bode plot and (**b**) Nyquist plot formats, recorded at different immersion periods: 5, 24, 72, 120, and 168 h.

It is understood that, through EIS measurements, a differential electrical pulse induces the movement of aligned electric dipoles within the polymer structure. These dipoles can reorient their position, facilitating polarization at the interface. This allows electron charge accumulation at the membrane interface when it is implanted in a biological environment, a property essential in biomaterials. The impedance diagrams indicate that longer exposure time in the physiological medium promotes more efficient polarization, allowing the membrane to better adapt to its environment. This dipole reorientation, accompanied by atomic or ionic disorder, suggests the possibility of mechanical deformation in the structure, leading to the manifestation of the piezoelectric effect. Currently, there are no specific references in the literature reporting the use of electrochemical techniques, particularly electrochemical impedance spectroscopy (EIS), to analyze the electric potential behavior of PVDF polymer material.

3.6.4. Electrical Circuit Modeling

In Figure 12, an equivalent electrical circuit (ECC) model is proposed to simulate the interfacial mechanisms by using a combination of resistors and capacitors connected in series or parallel, depending on the surface conditions. The configurations are based on the concept of an RC network. However, their complexity may vary; five circuits are configured using R and C element combinations to model the physical and chemical processes occurring at the material/electrolyte interface. This validation approach ensures the samples' structural and electrochemical integrity as a biomaterial with the possibility of functioning as a regenerative scaffold. The theoretical impedance response of the fitted circuit is represented in the Nyquist plot of Figure 12a for the circuit configuration of R(CR), which produces a well-defined semicircle shape. This semicircle response is characteristic of charge transfer resistance (R_{ct}), and its diameter directly measures R_{ct}. For the EIS system modeled using the R(CR)(CR) equivalent circuit, shown in Figure 11b, the simulated data plot shows the imaginary impedance component (Z″) against the real impedance component (Z′), allowing the identification of three different electrochemical behaviors; curve 1 corresponds to a system with lower impedance values, curve 2 represents an intermediate impedance response, and curve 3 exhibits the highest impedance response. The corresponding simulation data are summarized in Table 4.

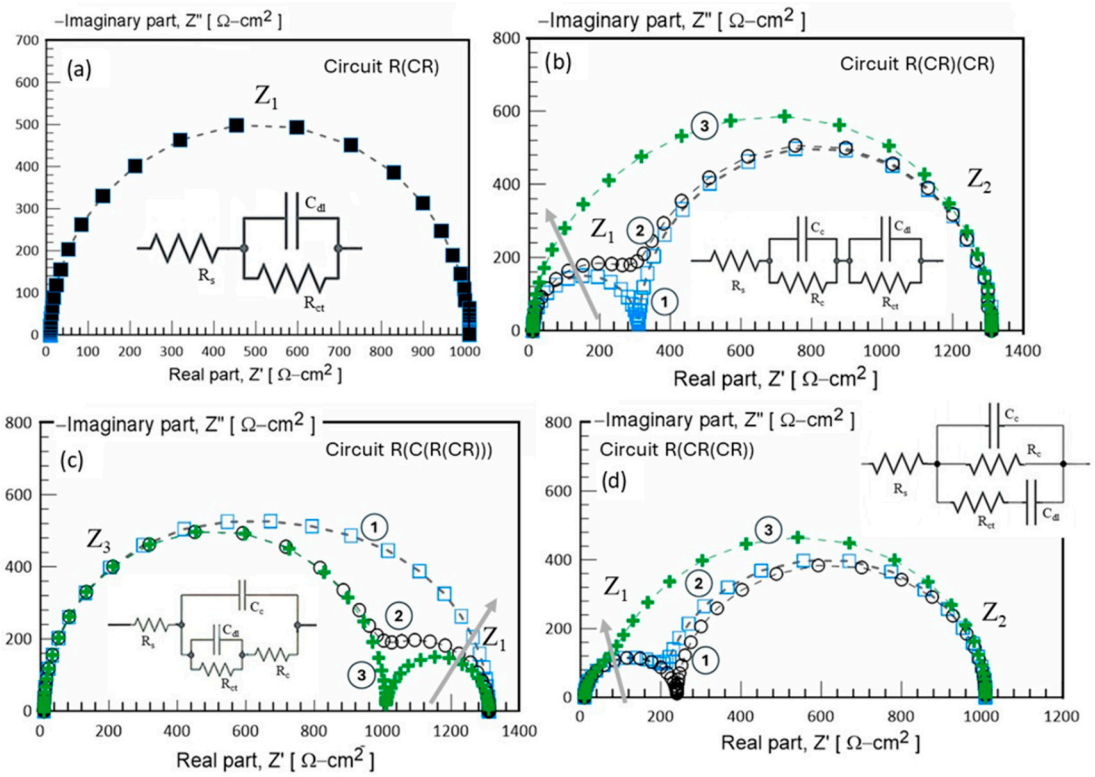

Figure 12. Equivalent electrical circuit (EEC) used to model the impedance behavior of biomaterial after 168 h of exposure in a 0.9% NaCl solution. R_s: solution resistance; C_c: coating capacitance; R_{ct}: charge transfer resistance; Q: constant phase element (CPE). (**a**) R(CR) model, (**b**) R(CR)(CR) model, (**c**) R(C(R(RC))) model, and (**d**) R(RC(CR)).

Table 4. Electrochemical parameters obtained from the fitting procedure of EIS data using the equivalent electrical circuit ECC proposed in Figure 9.

Data	Circuit R(CR)	Circuit R(CR)(CR)			Circuit R(C(R(CR)))			Circuit R(CR(CR))		
Modelling		1	2	3	1	2	3	1	2	3
R_s [Ω-cm^2]	10		10			10			10	
C_c [F/cm^2]	-	1×10^{-6}	1×10^{-5}	1×10^{-4}	1×10^{-6}	1×10^{-6}	1×10^{-6}	1×10^{-6}	1×10^{-5}	1×10^{-4}
R_c [Ω-cm^2]	-		300			300			300	
C_{ct} [F/cm^2]	1×10^{-5}	1×10^{-3}	1×10^{-4}	1×10^{-4}	1×10^{-2}	1×10^{-4}	1×10^{-5}	1×10^{-4}	1×10^{-4}	1×10^{-5}
R_{ct} [Ω-cm^2]	1000		1000			1000			1000	

The EIS results clearly reveal two time constants in curves 1 and 2, which correspond to the arrangement of the proposed ECC. The first semicircle (Z_1), which appears at lower Z′ values, is attributed to the RC pair (R_c, C_c), representing surface reactions such as ion adsorption on thin-layer interactions. The second semicircle (Z_2) at higher Z′ values is related to the RC pair (R_{ct}, C_{dl}), suggesting the bulk charge transfer resistance and ion diffusion processes within the material. However, an increase in the capacitance value (C_c) from 1×10^{-6} to 1×10^{-4} F/cm^2 results in significant ion accumulation at the interface, leading to a transition from two distinguishable semicircles to a single semicircle response, as observed in curve 3. Figure 12a–d, display the simulated EIS data using various RC configurations. Despite differences in their structural complexity, these equivalent circuits exhibit similar impedance behavior, demonstrating the effectiveness of the proposed modeling approach. Due to the similar characteristics between the experimental EIS data and the simulated EIS response using circuit R(CR(CR)) (Figure 12d), this model is identified as the most appropriate for evaluating the electrochemical impedance behavior of the PVDF membrane. Circuit R(CR(CR)) effectively represents the complex interfacial phenomena oc-

curring within the membrane/electrolyte system. PVDF membranes often exhibit multiple interfacial processes, including charge transfer, ion diffusion, and dielectric polarization. By incorporating multiple R(C) units connected in series and parallel, the circuit R(CR(CR)) is capable of modeling the distinct electrochemical processes occurring at different frequencies. Its configuration allows for a more precise modeling of the frequency-dependent impedance characteristics observed in experimental measurements. Furthermore, circuit R(RC(CR)) Figure 12d provides an improved fit to the Nyquist plots obtained from EIS data, accounting for multiple time constants associated with the different electrochemical processes occurring at various frequency ranges. This improves the reliability of the extracted parameters, such as charge transfer resistance (R_{ct}) and double-layer capacitance (C_{dl}), thus enabling a more accurate assessment of the electrochemical performance and interfacial behavior of the PVDF membrane.

The electrochemical parameters associated with the passive surface (biofilm) can be obtained by modeling the experimental data using an equivalent electrical circuit (EEC), as proposed in Figure 13. This ECC describes the electrical interactions between Hep-G2 cells and the PVD substrate. The circuit arrangement (d) is modified by introducing a complex element, specifically a constant phase element (CPE), to fit the non-ideal behavior interface better. In this modified circuit, a solution resistance (R_s) is connected in series with a resistance (R_c) representing the resistance of the biofilm formed on the PVDF surface. R_c is arranged in parallel with a constant phase element (CPE-Q_1), which relates to the electrical properties of the passive layer. Subsequently, these elements are connected in parallel to a resistor that characterizes the charge transfer resistance through the passive surface–electrolyte double-layer interface, which is further connected in series to a second constant phase element (CPE-Q_2). Instead of an ideal capacitor, CPE accounts for the non-ideal capacitive behavior typically observed in heterogeneous biofilm surfaces. Additionally, Figure 13 also shows a schematic illustration representing the interaction between Hep-G2 cells and the PVDF surface as analyzed through electrochemical impedance spectroscopy. The electrochemical parameter values obtained from the corresponding Nyquist diagrams are summarized in Table 5.

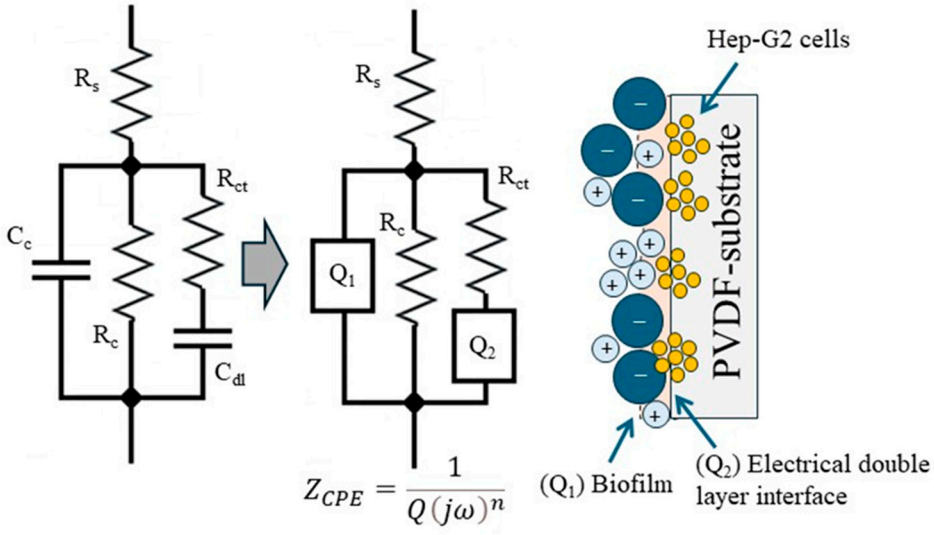

Figure 13. Equivalent electrical circuit (EEC) used to model the electrochemical response of a PVDF membrane in contact with Hep-G2 cells exposed for 168 h in 0.9% NaCl. R_s: solution resistance; Q_1: biofilm capacitance; R_c: biofilm resistance; Q: double-layer capacitance; R_{ct}: charge transfer resistance.

Table 5. Electrochemical parameters obtained during the fitting procedure of EIS data with the equivalent electrical circuit ECC proposed in Figure 13.

Data	Exposure Time in NaCl 0.9%Wt.				
	5 h	**24 h**	**72 h**	**120 h**	**168 h**
R_s [Ω]	9.24	9.47	9.15	9.07	9.7
Q_1 [S-sec^n]	1.035×10^{-9} (n = 0.9)	4.09×10^{-6} (n = 0.7)	2.00×10^{-6} (n = 0.6)	1.16×10^{-5} (n = 0.6)	8.07×10^{-5} (n = 0.6)
ω_{ref}-Q_1 [Hz]	159 kHz	6.31 Hz	6.34 Hz	6.34 Hz	4.0 Hz
R_1 [Ω]	5.79×10^4	3.00×10^4	1.78×10^4	1.58×10^4	1.126×10^4
Q_2 [S-sec^n]	4.37×10^{-7} (n = 0.8)	2.288×10^{-6} (n = 0.8)	4.39×10^{-5} (n = 0.7)	4.77×10^{-4} (n = 0.6)	2.97×10^{-4} (n = 0.6)
ω_{ref}-Q_2 [Hz]	1.26 Hz	5.04 Hz	6.34 mHz	252 mHz	252 mHz
R_2 [Ω]	6908	3197	1386	1136	63.43
Chi-square	5.58×10^{-4}	9.58×10^{-4}	1.04×10^{-4}	2.45×10^{-4}	1.40×10^{-4}

According to references [36–42], it is demonstrated that in electrochemical impedance spectroscopy (EIS) measurements, experimental EIS data can be used correctly by using an electrical circuit model that incorporates a constant phase element (CPE). The CPE is employed to model the non-ideal capacitive behavior caused by factors such as surface roughness, inhomogeneities, or diffusion effects. Unlike an ideal capacitor, which exhibits a purely capacitive response, a CPE displays a frequency-dependent impedance behavior described by the following equation:

$$Z_{CPE} = \frac{1}{Q(j\omega)^{-n}} \tag{8}$$

where Z_{CPE} is the impedance of the CPE, Q is the CPE constant magnitude in $\Omega^{-1}\cdot$sn, j is the imaginary unit $(j^2 = -1)$, ω is the angular frequency $(\omega = 2\pi f)$, f in Hz, and n $(0 \leq n \leq 1)$ is the phase constant exponent related to deviation from ideal capacitive behavior. The relationship between the CPE parameter Q and an equivalent capacitance C is given by the following equation:

$$C = Q\cdot\left(\omega_{ref}\right)^{n-1} \tag{9}$$

$$Z_4 = R_s + \frac{1}{\left(\frac{1}{R_{ct}} + (j\omega)^{n1}Q_1\right)} + \frac{1}{\left(\frac{1}{R_c} + (j\omega)^{n2}Q_2\right)} \tag{10}$$

where C represents the equivalent capacitance and ω_{ref} is a reference angular frequency $(\omega = 2\pi f)$ expressed in rad/s. When $(n = 1)$, the system behaves as a pure capacitor, and Q is directly equal to the capacitance C. However, if $(n < 1)$, the system deviates from ideal capacitive behavior, and the capacitance (C) becomes frequency dependent. Lower values of n indicate higher deviations, typically caused by surface roughness, inhomogeneities, or non-uniform charge distribution. It is necessary to apply this correction in electrochemical systems to obtain an accurate representation of capacitance from impedance measurements, and it must be normalized to the exposed surface area of 0.8 cm^2. The electrochemical parameters initially presented in Table 6 are recalculated to obtain new EIS data values, representing the electrochemical behavior of the system under study.

Finally, the results indicate that the ion adsorption and charge transfer mechanism through the pores of the PVDF polymeric membrane, which carries Hep-G2 cells, demonstrates excellent electrochemical stability and efficient ion interchange, promoting rapid biofilm formation. Additionally, the findings reveal good resistance to corrosion degradation during prolonged exposure time to physiological media, such as a 0.9% NaCl solution. The adsorption of Na^+, OH^-, PO_4^-, and Ca^+ ions promotes the film bioactivity of the surface, as indicated by the open-circuit potential activation without interface disturbance at the interface. In medical applications, particularly as a scaffold for tissue repair, this ion

adsorption capability facilitates the successful formation of biofilms on the bone, allowing for cellular osseointegration by providing active sites for the formation of the β-phase in the PVDF structure. The electrochemical findings from this study demonstrate the biomaterial's ability to adsorb ions at active sites associated with Hep-G2 cells and within its pores. This hydration mechanism is crucial for inducing the formation of an active biofilm interface, facilitating osteoconductive and tissue regeneration.

Table 6. Electrochemical parameters obtained from fitting EIS data using the equivalent electrical circuit ECC proposed in Figure 13.

Data	Exposure Time in NaCl 0.9%Wt.				
	5 h	**24 h**	**72 h**	**120 h**	**168 h**
R_s [Ω-cm^2]	9.24	9.47	9.15	9.07	9.7
C_c [F/cm^2]	2.64×10^{-10}	1.423×10^{-6}	5.06×10^{-6}	2.937×10^{-5}	2.66×10^{-5}
R_c [Ω-cm^2]	5.79×10^{4}	3.00×10^{4}	1.78×10^{4}	1.58×10^{4}	1.126×10^{4}
C_{dl} [F/cm^2]	2.956×10^{-7}	1.134×10^{-6}	1.422×10^{-5}	3.834×10^{-4}	2.388×10^{-4}
R_{ct} [Ω-cm^2]	6908	3197	1386	1136	63.43

4. Conclusions

PVDF membranes, fabricated by electrospinning using a home-built apparatus, exhibited uniform fiber morphology and well-defined structural features under controlled conditions. As demonstrated in this study, polyvinylidene difluoride (PVDF) emerges as a versatile polymer with excellent potential for biomedical applications, attributed to its remarkable thermal and chemical stability, inherent biocompatibility, and distinctive piezoelectric properties. Among its various crystalline configurations, the β-phase is characterized by its polar orientation, which is particularly desirable for tissue engineering applications due to its highest piezoelectric response. Hep-G2 cells were effectively cultured on PVDF membranes, which were adapted to the laboratory conditions. Experimental evidence confirmed that the PVDF fiber supported healthy cellular adhesion and proliferation, comparable to conventional plastic culture substrates.

This study demonstrated that electrospinning is an effective and reliable technique for producing PVDF membranes with active nanoparticles, offering promising applications in tissue engineering. The process enables the fabrication of electroactive materials with a predominant polar β-phase structure, which is essential for enhancing the piezoelectric properties of the resulting membranes. PVDF membranes exhibited excellent biocompatibility with Hep-G2 cells, as the cells adhered well, proliferated, and grew in a thermodynamically favorable manner on the membrane interface, without inducing any contamination or abnormal morphological alterations during the culture period. Among the tested substrates, notable differences in cellular preference were observed; cells cultured on glass exhibited limited proliferation, whereas cells cultured on PVDF membranes demonstrated adequate adhesion and confluence. However, cells maintained a preferential adhesion to the standard plastic container.

The EIS technique was employed to evaluate the electroactive response of the PVDF membranes, confirming their suitability for supporting the adhesion and proliferation of Hep-G2 cells. Furthermore, the performance of these membranes was found to be just as effective as standard polymeric substrates in promoting Hep-G2 cell culture, demonstrating their ability to interact with the biological system for cellular regeneration.

Cell adhesion and membrane interface: Initially, the PVDF membrane exhibits a characteristic impedance response when immersed in a 0.9% NaCl solution, resulting from its dielectric and interfacial properties. As Hep-G2 cells begin to adhere to the membrane surface, they probably form a biological film that alters the impedance spectra.

In particular, increases in charge transfer resistance (R_{ct}) and double-layer capacitance (C_{dl}) related to the electron charge are observed. These changes are attributed to the polarization of the cells and their electrostatic interactions with the polar β-phase of the PVDF membrane. This interaction facilitates the mobility of electrical charges and ionic species at the membrane interface, indicating electrobiological activity associated with the formation of a bio-interface.

Cell proliferation and surface coverage: As the immersion time progresses, cell proliferation results in increased surface coverage, which leads to significant changes in impedance characteristics. A notable decrease in R_{ct} suggests enhanced cell attachment and the formation of a conductive biofilm, which facilitates electron charge. Simultaneously, variations in capacitance electron charge (C_{dl}) may be associated with changes in the dielectric constant of the cells. This establishes an effective mechanism for electrical interaction between the cell-covered membrane surface and the surrounding electrolyte.

Biocompatibility assessment: The biocompatibility of the PVDF membrane is evaluated by examining the impedance spectra over time. A progressive change over time of impedance parameters indicates healthy cell growth and constant adhesion to the membrane surface. On the other hand, when the ionic charging process predominates at the membrane–electrolyte interface and cellular attachment still occurs, a decrease in R_{ct} and an increase in C_{dl} were observed. These changes are consistent with the biocompatibility response and reflect the dynamic physicochemical interactions occurring during initial cell–surface contact. In summary, the electrochemical behavior suggests that ionic transport and the accumulation of electron charge at the PVDF membrane interface contribute to the formation of a stable bio-interface, which is promising for cellular attachment and long-term proliferation in a physiological environment.

The presented study contributes to the use of electrochemical impedance spectroscopy (EIS) as a fundamental and versatile characterization technique to evaluate interfacial properties, charge transfer behavior, and bioelectrical responses in advanced biomaterials.

Author Contributions: Conceptualization, C.O.G.M. and J.d.J.A.F.C.; methodology, C.O.G.M., J.d.J.A.F.C. and H.H.H.; formal analysis C.O.G.M., J.d.J.A.F.C. and H.H.H.; investigation, C.O.G.M., J.d.J.A.F.C., H.H.H., G.L.H. and I.Z.R.-L.; resources, C.O.G.M., J.d.J.A.F.C., H.H.H., C.J.T.R. and J.A.A.C.; data curation, C.O.G.M., J.d.J.A.F.C., H.H.H., G.L.H. and I.Z.R.-L.; writing—original draft preparation, C.O.G.M., J.d.J.A.F.C. and H.H.H.; writing—review and editing, C.O.G.M., J.d.J.A.F.C. and H.H.H.; visualization, C.O.G.M., J.d.J.A.F.C., H.H.H., C.J.T.R., G.L.H. and J.A.A.C.; supervision, C.O.G.M., J.d.J.A.F.C., H.H.H., C.J.T.R. and J.A.A.C.; project administration, C.O.G.M. and J.d.J.A.F.C.; funding acquisition, C.O.G.M. and J.d.J.A.F.C. All authors have read and agreed to the published version of the manuscript.

Funding: This research received no external funding.

Institutional Review Board Statement: Not applicable.

Informed Consent Statement: Not applicable.

Data Availability Statement: The data supporting this study's findings cannot be made freely available. Requests for access to the presented data should be made to the corresponding author.

Acknowledgments: The authors thank the Universidad Autónoma del Estado de México, campus Valle de México, for the facilities provided to work in their laboratories. JJA Flores Cuautle acknowledges the UAEMex for the facilities provided at CU UAEM Valle de México, which enabled him to carry out his sabbatical research stay between 2023 and 2024. 3H (Héctor Herrera Hernández), C. O. González, G. Lara Hernandez, and J.J.A. Flores gratefully acknowledge the monthly stipend and continuous recognition granted by the Mexican National System of Researchers (SNII). The authors also sincerely appreciate the valuable contributions of collaborators and students involved in experimental work and data analysis, whose efforts were invaluable to the completion of this

research study. 3H respectfully dedicates this work to the memory of Florian Mansfeld and Digby D. Macdonald, whose pioneering contributions to the fields of electrochemistry, corrosion science, and materials protection continue to inspire generations of researchers. Their profound scientific legacy, unwavering commitment to excellence, and mentorship have had a lasting impact on the global scientific community.

Conflicts of Interest: The authors declare no conflicts of interest.

References

1. Theocharis, A.D.; Skandalis, S.S.; Gialeli, C.; Karamanos, N.K. Extracellular matrix structure. *Adv. Drug Deliv. Rev.* **2016**, *97*, 4–27. [CrossRef]
2. Rothman, S. How is the balance between protein synthesis and degradation achieved? *Theor. Biol. Med. Model.* **2010**, *7*, 25. [CrossRef]
3. Ribeiro, C.; Correia, D.M.; Lanceros-Méndez, S. Piezoelectric polymers as biomaterials for tissue engineering applications. *Colloids Surf. B Biointerfaces* **2015**, *136*, 46–55. [CrossRef] [PubMed]
4. Jacob, J.; More, N.; Kalia, K.; Kapusetti, G. Piezoelectric smart biomaterials for bone and cartilage tissue engineering. *Inflamm. Regen.* **2018**, *38*, 2. [CrossRef] [PubMed]
5. Chen, G.; Ushida, T.; Tateishi, T. A biodegradable hybrid sponge nested with collagen microsponges for dermal tissue engineering. *Biomaterials* **2002**, *23*, 2447–2453. [CrossRef]
6. Martins, P.; Lopes, A.C.; Lanceros-Méndez, S. Electroactive phases of poly(vinylidene fluoride): Determination, processing and applications. *Prog. Polym. Sci.* **2014**, *39*, 683–706. [CrossRef]
7. Dallaev, R.; Pisarenko, T.; Sobola, D.; Orudzhev, F.; Ramazanov, S.; Trčka, T. Brief review of PVDF properties and applications potential. *Polymers* **2022**, *14*, 4793. [CrossRef]
8. Li, Y.; Liao, C.; Tjong, S.C. Electrospun polyvinylidene fluoride-based fibrous scaffolds with piezoelectric characteristics for bone and neural tissue engineering. *Nanomaterials* **2019**, *9*, 952. [CrossRef] [PubMed]
9. Ribeiro, C.; Sencadas, V.; Botelho, G.; Lanceros-Méndez, S. Tailoring the morphology and crystallinity of poly(vinylidene fluoride) in electrospun nanofibers. *J. Nanomater.* **2015**, *2015*, 015001.
10. Zhang, Y.; Martínez-Gómez, A.; Li, X.; Pérez, M.A. Polyvinylidene fluoride in biomedical applications: Properties, challenges, and future prospects. *Eur. Polym. J.* **2025**, *231*, 113889. [CrossRef]
11. Sajkiewicz, P.; Wasiak, A.; Gocłowski, Z. Phase transitions during stretching of poly(vinylidene fluoride). *Eur. Polym. J.* **1999**, *35*, 423–429. [CrossRef]
12. Wang, Y.; Zhu, L.; Du, C. Progress in piezoelectric nanogenerators based on PVDF composite films. *Micromachines* **2021**, *12*, 1278. [CrossRef]
13. Lim, J.Y.; Kim, S.; Seo, Y. Enhancement of β-phase in PVDF by electrospinning. *AIP Conf. Proc.* **2015**, *1664*, 070006. [CrossRef]
14. Zhao, Y.; Lei, Y.; Zhang, L. Electrospun PVDF-based piezoelectric nanofibers: Materials, structures, and applications. *Nanoscale Adv.* **2023**, *5*, 1043–1059. [CrossRef]
15. Yin, J.; Boaretti, C.; Lorenzetti, A.; Trivellin, N.; Modesti, M.; Roso, M. Piezoelectric field enhanced photocatalytic efficiency of PVDF/TiO_2 core–shell nanofibrous membrane via coaxial electrospinning. *J. Environ. Chem. Eng.* **2023**, *11*, 110298. [CrossRef]
16. Pusty, M.; Sinha, L.; Shirage, P.M. A flexible self-poled piezoelectric nanogenerator based on a rGO–Ag/PVDF nanocomposite. *New J. Chem.* **2019**, *43*, 284–294. [CrossRef]
17. Bagla, A.; Mitharwal, C.; Rault, F.; Salaün, F.; Mitra, S. Influence of solution parameters on phase formation and morphology of electrospun poly(vinylidene fluoride) nanofiber. *arXiv* **2022**. [CrossRef]
18. Mohammadpourfazeli, S.; Arash, S.; Ansari, A.; Yang, S.; Mallick, K.; Bagherzadeh, R. Future prospects and recent developments of polyvinylidene fluoride (PVDF) piezoelectric polymer; fabrication methods, structure, and electromechanical properties. *RSC Adv.* **2023**, *13*, 370–387. [CrossRef]
19. Sharma, T.; Aroom, K.; Naik, S.; Gill, B.; Zhang, J.X.J. Flexible thin-film PVDF-TrFE based pressure sensor for smart catheter applications. *Ann. Biomed. Eng.* **2013**, *41*, 744–751. [CrossRef] [PubMed]
20. Saxena, P.; Shukla, P. A comparative analysis of the basic properties and applications of poly (vinylidene fluoride)(PVDF) and poly (methyl methacrylate)(PMMA). *Polym. Bull.* **2022**, *79*, 5635–5665. [CrossRef]
21. Tandon, B.; Magaz, A.; Balint, R.; Blaker, J.J.; Cartmell, S.H. Electroactive biomaterials: Vehicles for controlled delivery of therapeutic agents for drug delivery and tissue regeneration. *Adv. Drug Deliv. Rev.* **2018**, *129*, 148–168. [CrossRef]
22. Zhang, J.; Liu, X.; Jiang, Y. Advanced functional polymer materials for biomedical applications. *J. Appl. Polym. Sci.* **2023**, *140*, e56391. [CrossRef]
23. Liu, Y.; Li, J.; Yao, J. Polymeric membranes for biomedical applications. *Polymers* **2022**, *15*, 619. [CrossRef]

24. Motamedi, A.S.; Mirzadeh, H.; Hajiesmaeilbaigi, F.; Bagheri-Khoulenjani, S.; Shokrgozar, M. Effect of electrospinning parameters on morphological properties of PVDF nanofibrous scaffolds. *Prog. Biomater.* **2017**, *6*, 113–123. [CrossRef] [PubMed]
25. Makarov, V.A.; Makarova, L. Dependence and homeostasis of membrane impedance on cell morphology. *Sci. Rep.* **2018**, *8*, 10314. [CrossRef] [PubMed]
26. Li, H.; Tian, X.; Sun, X.; Zhang, Y.; Wang, H. Piezoelectric biomaterials for innovative regenerative medicine. *Adv. Healthc. Mater.* **2019**, *8*, 1801043. [CrossRef]
27. Bai, Y.; Wang, X.; Zhao, Y.; Li, D. Piezoelectric materials for biomedical applications. *Mater. Today Phys.* **2021**, *20*, 100460. [CrossRef]
28. Dagdeviren, C.; Su, Y.; Joe, P.; Yona, R.; Liu, Y.; Kim, Y.-S.; Huang, Y.Y.; Damadoran, A.R.; Xia, J.; Martin, L.W.; et al. Conformal piezoelectric energy harvesting and storage from motions of the heart, lung, and diaphragm. *Nat. Commun.* **2014**, *5*, 4496. [CrossRef]
29. Wang, Z.L. On Maxwell's displacement current for energy and sensors: The origin of nanogenerators. *Mater. Today* **2017**, *20*, 74–82. [CrossRef]
30. López Juárez, C.X. Aplicación de la Tecnología de Electrospinning Para el Desarrollo de la Mejora Continua de la Producción Industrial. Master's Thesis, Universidad Autónoma del Estado de México, Repositorio Institucional de la UAEMEX, Toluca, Mexico, 2024.
31. Alberts, B. *Molecular Biology of the Cell*; Garland Science: New York, NY, USA, 2017.
32. Segeritz, C.-P.; Vallier, L. Cell Culture: Growing Cells as Model Systems in vitro. In *Basic Science Methods for Clinical Researchers*; Elsevier: Amsterdam, The Netherlands, 2017; pp. 151–172.
33. Porras-Herrera, D.R.; Herrera-Hernández, H.; Miranda-Hernández, J.G.; Castillo-Robles, J.A.; Armendariz-Mireles, E.N.; Calles-Arriaga, C.A.; Rocha-Rangel, E. Innovative bioceramic based on hydroxyapatite with titanium nanoparticles as reinforcement for possible medical applications. *J. Manuf. Mater. Process.* **2024**, *8*, 296. [CrossRef]
34. Herrera Hernández, H.; Mandujano Ruiz, A.; González Morán, C.O.; Miranda Hernández, J.G.; Flores Cuautle, J.d.J.A.; Morales Hernández, J.; Hernández Casco, I. Microstructural and Electrochemical Study: Pitting Corrosion Mechanism on A390 Al–Si Alloy and Ce–Mo Treatment as a Better Corrosion Protection. *Materials* **2024**, *17*, 3044. [CrossRef] [PubMed]
35. Herrera Hernández, H.; Ruiz Reynoso, A.M.; Trinidad González, J.C.; González Morán, C.O.; Miranda Hernández, J.G.; Mandujano Ruiz, A.; Morales Hernández, J.; Orozco Cruz, R. Electrochemical Impedance Spectroscopy (EIS): A Review Study of Basic Aspects of the Corrosion Mechanism Applied to Steels. In *Electrochemical Impedance Spectroscopy*; IntechOpen: Rijeka, Croatia, 2020. [CrossRef]
36. Mansfeld, F.; Hsu, C.-H. Technical note: Concerning the conversion of the constant phase element parameter Y_0 into a capacitance. *Corrosion* **2001**, *57*, 747–748. [CrossRef]
37. Mansfeld, F.; Hsu, C.-H. On the physical interpretation of constant phase elements. *Electrochem. Solid-State Lett.* **2001**, *4*, B1–B3.
38. Mansfeld, F.; Hsu, C.-H. On the intrinsic coupling between constant-phase element parameters α and Q in electrochemical impedance spectroscopy. *Electrochem. Solid-State Lett.* **2001**, *4*, B67–B69.
39. He, Z.; Mansfeld, F. Exploring the use of electrochemical impedance spectroscopy (EIS) in microbial fuel cell studies. *Energy Environ. Sci.* **2009**, *2*, 215–219. [CrossRef]
40. Brug, G.J.; Van den Eeden, A.L.G.; Sluyters-Rehbach, M.; Sluyters, J.H. The analysis of electrode impedances complicated by the presence of a constant phase element. *J. Electroanal. Chem. Interfacial Electrochem.* **1984**, *176*, 275–295. [CrossRef]
41. Hirschorn, B.; Orazem, M.E.; Tribollet, B.; Musiani, M. Determination of effective capacitance and film thickness from constant-phase-element parameters. *Electrochim. Acta* **2010**, *55*, 6218–6227. [CrossRef]
42. Palomar-Pardavé, M.; Romero-Romo, M.; Herrera-Hernández, H.; Abreu-Quijano, M.A. Influence of the alkyl chain length of 2-amino-5-alkyl-1,3,4-thiadiazole compounds on the corrosion inhibition of steel immersed in sulfuric acid solutions. *Corros. Sci.* **2012**, *54*, 231–243. [CrossRef]